理學博士 學位論文

시상하부 에너지대사 조절 뉴론의 활성 조절 기전 연구

Study for regulatory mechanism of hypothalamic neuronal activity for energy metabolism

蔚 山 大 學 校 大 學 院

生 命 科 學 科

金 光 坤

시상하부 에너지대사 조절 뉴론의 활성 조절 기전 연구

指 導 敎 授 李 炳 柱

이 論文을 理學博士 學位論文으로 提出함

2020 年 8 月

蔚 山 大 學 校 大 學 院

生 命 科 學 科

金 光 坤

김광곤의 이학박사학위 논문을 인준함

심 사 위 원 장 _____ 박 정 우 _____ 인

심 사 위 원 _____ 백 승 훈 _____ 인

심 사 위 원 _____ 하 창 만 _____ 인

심 사 위 원 _____ 김 재 근 _____ 인

심 사 위 원 _____ 이 병 주 _____ 인

울 산 대 학 교 대 학 원

2020년 8월

Study for regulatory mechanism of hypothalamic neuronal activity for energy metabolism

Supervisor: Byung Ju Lee, Ph.D

A Dissertation

Submitted to
the Graduate School of the University of Ulsan
in partial Fulfillment of the Requirements
for the Degree of

Doctor of Philosophy

by

Kim, Kwang Kon

Department of Biological science
Graduate School
University of Ulsan

August 2020

CONTENTS

Study for regulatory mechanism of hypothalamic neuronal activity for energy metabolism

CHAPTER 1

Function of astrocyte MyD88 in high-fat-diet-induced hypothalamic inflammation

Abstract

A growing body of evidences has been made identifying the hypothalamic inflammation that leads to the initiation of obesity development. In particular, the reactive gliosis accompanied with the inflammatory responses in hypothalamus is the pivotal cellular event that elicits the metabolic abnormalities. In this study, I evaluated whether MyD88 signaling in hypothalamic astrocytes is deeply involved in the obesity pathogenesis through mediating inflammatory responses utilizing a mouse line bearing ablation of *MyD88* gene in astrocyte specifically. The mice displayed reduced hypothalamic inflammation in response to treatment of a saturated free fatty acid and a long-term exposure to fat rich diet. In line with these observations, I successfully blunted obesity development in astrocyte-specific MyD88 deficient mice. Intriguingly, I further identified that the mice displayed improved the leptin resistance induced by a long-term HFD treatment. Collectively, current study suggested that MyD88 signaling in hypothalamic astrocytes is a critical molecular mediator on obesity pathogenesis triggered by hypothalamic inflammation.

Introduction

The increasing rate of obesity in the global population has become a major public health problem. Therefore, many investigations have been performed to identify the underlying mechanisms and pathological components of obesity [1, 2]. In particular, it has been proposed that perturbation of the hypothalamic neuronal circuit that controls whole-body energy metabolism is a primary cause of obesity development [3-5]. During the past decade, a great deal of attention has been paid to investigating the hypothalamic neuronal circuit linked to whole-body energy metabolism under the control of afferent inputs derived from metabolically involved peripheral organs [6-8].

Astrocytes are the most abundant cells in the central nervous system and dynamically participate in maintaining normal neuronal functions by playing multiple supportive roles. Thus, a growing body of evidence has emerged linking metabolic processes in hypothalamic astrocytes with the physiological or pathological control of body energy balance [9-11]. According to the recent literature, neuroinflammation and reactive gliosis can be observed in the hypothalami of mice exposed to a high-fat diet (HFD) before the occurrence of significant body weight gain, and this is sustained with continuous HFD feeding, suggesting that hypothalamic gliosis accompanied by inflammation is a crucial cellular event in obesity pathogenesis [12-15]. Thus, unmasking the underlying mechanism by which an HFD induces hypothalamic inflammation and gliosis is required to better understand the initiation and deterioration of metabolic disorders caused by over-nutrition.

Myeloid differentiation primary response 88 (MyD88) is a crucial adaptor molecule of Toll-like receptor (TLR) signaling that initiates innate immunity by mediating a variety

of humoral factors and infectious pathogens [16-18]. In particular, the TLR and MyD88 axis in the hypothalamus is a key player in HFD–induced hypothalamic inflammatory responses. Mice fed with an HFD expressed high levels of TLR4 and MyD88 in the hypothalamus, which was coupled with intracellular inflammatory signaling cascades such as the Jun kinase and nuclear factor kappa B (NF-κB) pathways [19, 20]. A recent study reported that interaction between circulating saturated free fatty acids (sFFAs) and TLR4 was involved in the hypothalamic control of energy homeostasis and that mice bearing neuron-specific deletion of the *Myd88* gene were protected against HFD-induced obesity through the alleviation of hypothalamic inflammation and leptin resistance [21]. However, it is unclear whether TLR and MyD88 signaling in astrocytes is triggered by over-nutrition and thus directly linked to the development of obesity in association with hypothalamic gliosis and inflammation. In this study, I investigated whether MyD88 signaling in astrocytes is involved in hypothalamic inflammation and reactive gliosis and whether altering the activity of MyD88 signaling in astrocytes, using mutant mice bearing an astrocyte-specific deletion of *Myd88* gene expression, would affect the obesity phenotype and leptin resistance induced by HFD consumption.

Materials and Methods

Animals

Animals were fed a standard diet (STD, Feedlab, Gyeonggi-Do, Korea) or HFD (D12492, Research Diets, New Brunswick, NJ, USA) *ad libitum* and given free access to tap water. All animals were maintained in temperature- and humidity-controlled rooms with a 12 h/12 h light-dark cycle, with the lights on from 7:00 a.m. to 7:00 p.m. *Myd88* floxed (*Myd88*$^{fl/fl}$) mice (Stock No. 008888), glial fibrillary acidic protein *(Gfap)-CreER*^{T2} mice (Stock No. 012849), and *Ai14* reporter mice (Stock No. 007914) were purchased from Jackson Laboratory (Bar Harbor, ME, USA). *Myd88*$^{fl/fl}$ mice were crossbred with *Gfap-CreER*^{T2} mice to generate *Myd88* conditional knockout (KO) mice missing *Myd88* specifically in cells expressing GFAP (*Myd88*$^{\Delta GFAP}$). *Ai14* reporter mice were crossbred with *Gfap-CreER*^{T2} mice to label GFAP-positive astrocytes with tomato signals. Because the *Gfap-CreER*^{T2} mice expressed Cre recombinase under the control of the tamoxifen-inducible *GFAP* promoter, six-week-old *Myd88*$^{\Delta GFAP}$ mice and their littermate control (*Myd88*$^{fl/fl}$) mice received daily injections for 5 days of tamoxifen (100 mg/kg, T5648, Sigma-Aldrich, St. Louis, MO, USA) dissolved in corn oil (C8267, Sigma-Aldrich). All animals and procedures used were in accordance with the guidelines and approval of the Institutional Animal Care and Use Committee at the University of Ulsan (permission numbers: BJL-15-010, BJL-18-010, and BJL-19-010).

Ribo-Tag system

To analyze mRNA species that are specifically translated in hypothalamic astrocytes, we used the Ribo-Tag translational profiling system [22, 23]. In this study, I used

Rpl22^{HA} mice (Stock No. 011029, Jackson Laboratory), which have a *loxP*-flanked wild-type exon 4 followed by an identical exon 4 tagged with hemagglutinin (HA), as the Ribo-Tag animal. Crossbreeding Ribo-Tag mice with mice expressing Cre recombinase resulted in the deletion and replacement of the floxed wild-type exon 4 with the HA-tagged exon 4 in cells expressing Cre. The astrocyte-specific *Myd88* KO (*Myd88*$^{\Delta GFAP}$) mice were crossbred with *Rpl22*^{HA} mice to generate *Myd88*$^{\Delta GFAP}$*;Rpl22*^{HA} mice that had both the HA-tagged ribosomal protein Rpl22 and the deletion of Myd88 in astrocytes. The *Rpl22*^{HA} mice were also crossed with control *Myd88*$^{+/+}$-*Gfap-CreER*^{T2} (*Gfap-Cre*) mice, which resulted in control mice bearing an astrocyte-specific Ribo-Tag system (*Gfap-Cre;Rpl22*^{HA} mice).

RNA isolation with the Ribo-Tag system was conducted as previously described [22, 23]. Briefly, dissected hypothalamus samples were collected from animals and homogenized. RNA was extracted from 10% of the cleared lysate and used as input. The remaining lysate was incubated with mouse anti-HA antibody for 4 h at 4°C followed by the addition of protein G agarose beads (LGP-1018B, Lugen, Gyeonggi-Do, Korea) and overnight incubation at 4°C. The beads were washed three times in high salt solution. The bound ribosomes and RNA were separated from the beads with 30 sec of vortexing, and RNA was further purified using a QIAGEN RNeasy Micro Kit (74034, Qiagen, Hilden, Germany). After RNA isolation, I obtained 10–20 ng of RNA sample/hypothalamus. The RNA samples were then subjected to real-time PCR analysis.

Measurement of food intake and leptin administration

Five days before I began the food intake measurements, I moved the mice into individual cages and allowed them to acclimatize to their new environment. Food intake was measured for a week at 23-24 weeks of age during HFD feeding and calculated as an average daily food intake (Fig. 2A).

Body weight was measured every week during HFD feeding. To determine how leptin affected feeding behavior, mice were intraperitoneally (ip) injected with vehicle (saline) or recombinant mouse leptin (2 mg/kg; R&D Systems, Minneapolis, MN, USA) after overnight fasting. The food intake of the individually caged animals was monitored for 24 h after the injection, and then their body weights were measured.

Cannulation and administration of palmitic acid

For intracerebroventricular (icv) cannula implantation, mice were anesthetized by ip injection of tribromoethanol (250 mg/kg, Sigma-Aldrich) and placed in a stereotaxic apparatus (Stoelting, Wood Dale, IL, USA). The cannula (26 gauge) was implanted into the right lateral ventricle (1.0 mm lateral, 0.3 mm posterior, and 2.4 mm ventral to the bregma) according to the *Stereotaxic Mouse Brain Atlas* (Paxinos G and Franklin KBJ, 2001, Academic Press, San Diego, CA, USA) and secured to the skull with dental cement. After 7 days of recovery, the mice were injected with vehicle [5% bovine serum albumin (BSA)] and palmitic acid (50 pmol/2 μl, Sigma-Aldrich) dissolved in BSA solution. Mice were sacrificed 1 h after the injection of palmitic acid.

Administration of 5-bromodeoxyuridine

For the analysis of Iba1-positive cell proliferation upon HFD, mice received daily ip injections with 5-bromodeoxyuridine (BrdU, 100 mg/kg, Sigma-Aldrich) dissolved in saline for 5 days after HFD feeding for 8 weeks. On the 5th day of injection, mice were sacrificed 1 h after BrdU injection and their brain sections were analyzed with immunohistochemistry.

Immunohistochemistry (IHC)

Animals were deeply anesthetized with tribromoethanol and transcardially perfused with phosphate buffer (PB, 0.1 M, pH 7.4), followed by a fresh fixative of 4% paraformaldehyde in PB. Brains were post-fixed overnight at 4°C, sliced to a thickness of 50 μm using a vibratome (VT1000P; Leica Microsystems, Wetzlar, Germany), and then washed several times in PB. Coronal brain sections containing the hypothalamic arcuate nucleus (ARC) were preincubated with 0.2% Triton X-100 (T8787, Sigma-Aldrich) in PB for 30 min to permeabilize the tissues and cells. After further washing with PB, the sections were incubated overnight at room temperature (RT) with mouse anti-GFAP antibody (1:3,000; G3893, Sigma-Aldrich), rabbit anti-Iba1 antibody (1:3,000; 019-19741, Wako, Osaka, Japan), rabbit anti-pSTAT3 antibody (1:1,000; 9145, Cell Signaling Technology, Beverly, MA, USA), and mouse anti-HA antibody (1:1,000; MMS-101R, BioLegend, San Diego, CA, USA) or at 4°C with sheep anti-α-melanocyte stimulating hormone (MSH) antibody (1:10,000; AB5087, Millipore, Billerica, MA, USA). For BrdU staining, sections were incubated with 0.01 mol/L citrate buffer for 10 min at 80°C and washed in PB at RT. Sections were then incubated with

2 N HCl for 30 min and incubated with 0.2% Triton X-100 in PB for 30 min at RT. Afterward, sections were incubated with rat anti-BrdU antibody (1:200; ab74545, Abcam, Cambridge, MA, USA) overnight at RT. On the next day, sections were washed in PB. For immunofluorescence staining, sections were incubated with the following secondary antibodies for 2 h at room temperature: goat anti-rabbit Alexa Fluor 488 (1:500; A11008, Invitrogen, Carlsbad, CA, USA), goat anti-rabbit Alexa Fluor 594 (1:500; A11012, Invitrogen), chicken anti-rabbit Alexa Fluor 647 (1:500; A21443, Invitrogen), goat anti-mouse Alexa Fluor 488 (1:500; A11001, Invitrogen), goat anti-mouse Alexa Fluor 594 (1:500; A11005, Invitrogen), donkey anti-rat Alexa Fluor 594 (1:500; A21209, Invitrogen) and donkey anti-sheep Alexa Fluor 594 (1:500; A11016 , Invitrogen). Stained brain sections were imaged using an FV-1200 confocal laser-scanning microscope (Olympus America, Inc., Center Valley, PA, USA).

IHC image analyses

The number of immuno-positive cells in the hypothalamic ARC was counted by an unbiased observer. The intensity of immuno-positive cells was measured using ImageJ V 1.50 software (National Institutes of Health, Bethesda, MD). Region of interest (ROI) within an image was manually selected with the *Mouse Brain Atlas* for ARC or PVN (ARC: between -1.46 and -1.82 mm from bregma, PVN: between -0.82 and -1.06 mm from bregma). The images were converted to 8-bit images and threshold was applied. The images were binarized to separate the immuno-positive cells from the background. The fiber intensity and particle number of immuno-positive α-melanocyte stimulating hormone (α-MSH) signals in the PVN were measured using the ImageJ software. The size of Iba1-positive cells in the ARC was measured using

a thresholding parameter on ImageJ software as a previous report [24].

Blood glucose measurement

Blood glucose was measured with a glucometer (One Touch Ultra, LifeScan, Milpitas, CA, USA). For glucose tolerance tests (GTTs), mice were given an ip injection of D-glucose (1 g/kg) after overnight fasting. For insulin tolerance tests (ITTs), mice were fasted for 4 h before ip injection of human insulin (0.75 IU/kg). Blood glucose levels were determined from the tail vein at 0, 15, 30, 60, and 120 min after injection.

Measurement of O_2 consumption, CO_2 production, and energy expenditure

Metabolic parameters, O_2 consumption (VO_2), CO_2 production (VCO_2), and energy expenditure, of *MyD88*$^{fl/fl}$ and *MyD88*$^{\Delta GFAP}$ mice were analyzed using an indirect calorimetry system (Promethion, Sable Systems, Las Vegas, NV, USA). VO_2 and VCO_2 were measured at 10 min intervals for each mouse. Mice were acclimated in the chambers for 48 h prior to data collection. The average values during the light and dark periods were calculated. Data acquisition and instrument control were coordinated by MetaScreen software (version 2.3.12), and the obtained raw data were processed using ExpeData (version 1.9.14, Sable Systems).

Real-time PCR

RNA was isolated from hypothalami using Trizol reagent (Sigma-Aldrich) or immunoprecipitation with HA antibody, as explained above, and reverse transcribed with MMLV reverse transcriptase (Beams Biotechnology, Gyeonggi-do, Korea). Gene

expression was measured by real-time PCR using Evagreen qPCR Mastermix (TApplied Biological Materials Inc., Richmond, BC, Canada). The primers used were as follows: Myd88 sense primer, 5'-GCT ACT GCC CCA ACG ATA TC-3'; Myd88 antisense primer, 5'-ACA CAA CTT AAG CCG ATA GTC TG-3'; Il-1β sense primer, 5'-AGG GCT GCT TCC AAA CCT TTG AC-3'; Il-1β antisense primer, 5'-ATA CTG CCT GCC TGA AGC TCT TGT-3'; Il-6 sense primer, 5'-GAG ACT TCA CAG AGG ATA CCA C-3'; Il-6 antisense primer, 5'-TCT CAT TTC CAC GAT TTC CCA G-3'; Il-10 sense primer, 5'-TGG GTT GCC AAG CCT TAT CG-3'; Il-10 antisense primer, 5'-AAT CAC TCC TCA CCT GCT CCA CTG-3'; Tnf-α sense primer, 5'-TGG GAC AGT GAC CTG GAC TGT-3'; Tnf-α antisense primer, 5'-TTC GGA AAG CCC ATT TGA GT -3'; Gfap sense primer, 5'-CAG ACT TTC TCC AAC CTC CAG-3'; Gfap antisense primer, 5'-AAT CTG GTG AGC CTG TAT TGG-3'; Iba1 sense primer, 5'-TCT GCC GTC CAA ACT TGA AG-3'; Iba1 antisense primer, 5'-TCT AGG TGG GTC TTG GGA AC-3'; NeuN sense primer, 5'-ATG GTG CTG AGA TTT ATG GAG G-3'; NeuN antisense primer, 5'-CGA TGG TGT GAT GGT AAG GAT C-3'; β-actin sense primer, 5'-GAT CTG GCA CCA CAC CTT CT-3'; β-actin antisense primer, 5'-GGG GTG TTG AAG GTC TCA AA-3'; L19 sense primer, 5'-GGT GAC CTG GAT GAG AAG GA-3'; L19 antisense primer, 5'-TTC AGC TTG TGG ATG TGC TC-3'. Real-time PCR was performed using the StepOnePlus^{TM} Real-Time PCR System (Applied Biosystems, Foster City, CA, USA) for ~40 cycles. Relative mRNA expression was normalized with the β-actin or L19 mRNA level and calculated using the $2^{-\Delta\Delta CT}$ method [25].

Statistical analyses

Statistical analyses were performed in GraphPad Prism 5 software (GraphPad Software, San Diego, CA, USA). All data are expressed as the mean ± SEM. The statistical significance between two groups was analyzed by unpaired Student's t-test. Two-way analysis of variance (ANOVA) analyses followed by Bonferroni post-hoc testing were performed to detect the significance of differences between two genotypes.

Results

Myd88 gene expression in astrocytes was increased by long-term HFD feeding

To validate that long-term exposure to HFD caused reactive gliosis in the hypothalamus, mice were fed an HFD for 16 weeks, and IHC using antibodies against GFAP, a molecular marker for astrocytes, and Iba1, a marker for microglia, was performed with brain sections containing hypothalamic ARC (Fig. 1A, D). Consistent with previous reports [11, 12, 26], HFD feeding increased the number and intensity of GFAP-positive cells (Fig. 1B, C), and Iba1-positive cells (Fig. 1E, F).

To explore the function of MyD88 in hypothalamic astrocytes, I first used a Ribo-Tag system of transgenic (*Gfap-Cre;Rpl22*^{HA}) mice that expressed HA-tagged ribosomal protein Rpl22 in astrocytes to identify the *Myd88* mRNA species translated specifically in hypothalamic astrocytes. The IHC analysis identified specific HA signals in the GFAP-positive astrocytes (Fig. 1G). Real-time PCR using the Ribo-Tag system further revealed that HA-mediated immunoprecipitation occurred in the cells expressing GFAP, but not in those producing NeuN or Iba1 (Fig. 1H). The amount of *Myd88* mRNA translated in hypothalamic astrocytes was increased by HFD feeding (Fig. 1I), suggesting that astrocyte MyD88 could play a role in the response to over-nutrition.

Astrocyte-specific *Myd88* knockout alleviated HFD-induced hypothalamic gliosis

It has been well established that coupling between TLRs and MyD88 initiates innate immunity in several types of peripheral cells and is also involved in the hypothalamic

inflammatory responses linked to metabolic disorders [17, 18, 27]. To determine the effect of astrocyte MyD88 on HFD-induced astrogliosis and inflammation in the hypothalamus, I generated tamoxifen-inducible *Myd88* gene KO specifically in GFAP-positive cells (*Myd88*$^{\Delta GFAP}$). More than 83% of *Myd88* mRNA expression was eliminated in the hypothalamic astrocytes of *Myd88*$^{\Delta GFAP}$*;Rpl22*^{HA} mice, compared with that in the hypothalamic astrocytes of control *Gfap-Cre;Rpl22*^{HA} mice, as shown by a real-time PCR analysis of Ribo-Tag-purified mRNA (Fig. 2B).

Next, I measured the effect of this conditional *Myd88* KO on HFD-induced astrogliosis in the hypothalamic ARC by counting GFAP-immuno-positive signals (Fig. 2C). The HFD-induced increase in the number and intensity of GFAP-positive cells was completely offset by *Myd88* KO in astrocytes (Fig. 2D, E), suggesting the importance of MyD88 signaling in HFD-induced astrogliosis. The astrocyte-specific *Myd88* KO also inhibited the HFD-induced increase in the number, intensity and size of Iba1-positive cells in the hypothalamic ARC (Fig. 2F–I). Furthermore, the *Myd88* KO resulted in a decreased number of HFD-induced Iba1-positive cells that were incorporated with BrdU (Fig. 2J, K). These results suggested that astrocyte MyD88 signaling also participates in HFD-induced microglial proliferation and activation. Consistent with the decrease in HFD-induced astrogliosis in the mutant animals, astrocyte-specific *Myd88* KO decreased the HFD-induced mRNA expression of Gfap, Iba1 and proinflammatory cytokines in the hypothalamus (Fig. 2L). Real-time PCR analyses of hypothalamic mRNA purified with the Ribo-Tag system showed that astrocyte-specific *Myd88* KO decreased HFD-induced expression of proinflammatory cytokines Tnf-α and Il-1β, but did not significantly affect the HFD-induced anti-inflammatory cytokines in the hypothalamic astrocytes (Fig. 2M).

Astrocyte-specific *Myd88* KO affected hypothalamic gliosis triggered by palmitic acid

Because elevated levels of circulating sFFAs can cause hypothalamic reactive gliosis that is accompanied by inflammatory responses during over-nutrition [26, 28, 29], I next determined the effect of astrocyte-specific *Myd88* KO on the hypothalamic astrogliosis induced by the administration of palmitic acid, an sFFA. Palmitic acid induced an increase in the number and intensity of GFAP-positive astrocytes in the hypothalamic ARC, which was attenuated by *Myd88* KO in the astrocytes (Fig. 3A–C). Interestingly, astrocyte-specific *Myd88* KO also caused a similar effect on palmitic acid–induced increase in the number and intensity of Iba1-positive microglia (Fig. 3D–F). Taken together, the current findings suggest that MyD88 signaling is a crucial molecular mediator of the hypothalamic gliosis induced by an elevation in circulating sFFAs.

Astrocyte-specific *Myd88* KO did not affect metabolic phenotypes in the normal diet condition

Before I determined whether HFD-induced metabolic disorder could be ameliorated by specific *Myd88* KO in the astrocytes, I investigated the effect of astrocyte-specific *Myd88* KO on energy metabolism under the STD feeding condition. I examined alterations in metabolic parameters (food intake, body weight, and glucose metabolism) between the conditional KO ($Myd88^{\Delta GFAP}$) mice and control mice. The $Myd88^{\Delta GFAP}$

mice did not show any difference in food intake or body weight compared with control mice (Fig. 4A, B). Furthermore, the *Myd88*$^{\Delta GFAP}$ mice displayed normal glucose metabolism in the GTTs and ITTs (Fig. 4C–F). These results indicate that astrocyte-specific *Myd88* KO did not cause metabolic abnormalities in the STD condition.

Astrocyte-specific ablation of *Myd88* alleviated HFD-induced metabolic aggravation

To identify the pathological relevance of the reduced hypothalamic gliosis seen in the HFD-treated *Myd88*$^{\Delta GFAP}$ mice, both control and *Myd88*$^{\Delta GFAP}$ mice were fed an HFD for 16 weeks, and then their metabolic parameters were measured. The *Myd88*$^{\Delta GFAP}$ mice fed an HFD revealed a significant decrease in food intake and calorie intake compared with the HFD-fed control mice (Fig. 5A, B). Additionally, HFD-induced weight gain was significantly alleviated in the *Myd88*$^{\Delta GFAP}$ mice compared with control mice during the observation period (Fig. 5C). Along with the difference in body weight gain during HFD feeding, the peripheral metabolic organs, such as the liver and perirenal fat, of the *Myd88*$^{\Delta GFAP}$ mice weighted less than those of the control mice (Fig. 5D). Accordingly, the *Myd88*$^{\Delta GFAP}$ mice displayed improved glucose metabolism, as shown in GTTs and ITTs, after long-term exposure to HFD (Fig. 5E–H). To further investigate the effect of astrocyte-specific *Myd88* KO on energy expenditure, I measured multiple metabolic parameters using indirect calorimetry. The *Myd88*$^{\Delta GFAP}$ mice showed significant elevations of VO_2, VCO_2, and energy expenditure after long-term exposure to HFD, compared with control mice (Fig. 5I–M). Collectively, these observations demonstrate that selective ablation of the *Myd88* gene in astrocytes

ameliorates diet-induced obesity (DIO) and impaired glucose metabolism by affecting food intake and energy expenditure.

Astrocyte-specific deletion of the *Myd88* gene ameliorated long-term HFD feeding–induced leptin resistance

It has been well established that hypothalamic inflammation is a primary cause of leptin resistance, which is deeply associated with obesity pathogenesis. Therefore, I next investigated the responsiveness of the *Myd88*$^{\Delta GFAP}$ mice to leptin after 16 weeks of HFD feeding. An ip administration of leptin (2 mg/kg body weight) effectively reduced food intake and body weight in both control and *Myd88*$^{\Delta GFAP}$ mice fed a STD diet, indicating that astrocyte-specific *Myd88* KO did not affect leptin responsiveness under non-obesity conditions. Leptin-induced reduction in food intake and body weight disappeared completely in control (*Myd88*$^{fl/fl}$) mice fed an HFD for 16 weeks, indicating a condition of leptin resistance. However, *Myd88*$^{\Delta GFAP}$ mice fed an HFD for 16 weeks continued to display a decrease in food intake and body weight in response to leptin, indicating ameliorated leptin resistance (Fig. 6A, B).

Because phosphorylation of signal transducer and activator of transcription 3 (STAT3) is a cellular event that reflects the activation of leptin signaling, I determined leptin-induced STAT3 phosphorylation (pSTAT3) in the *Myd88*$^{\Delta GFAP}$ mice. The *Myd88*$^{\Delta GFAP}$ mice preserved leptin-induced pSTAT3 in the hypothalamic ARC after 16 weeks of HFD feeding, whereas the control mice lost the normalcy of leptin-induced pSTAT3 after long-term HFD feeding (Fig. 6C, D). Furthermore, leptin induced an increase in the number and intensity of α-MSH fibers in the paraventricular nucleus (PVN) of the *Myd88*$^{\Delta GFAP}$ mice after HFD feeding for 16 weeks, whereas it failed to

induce a significant change in the α-MSH fibers of the PVN of the control *Myd88*$^{fl/fl}$ mice (Fig. 6E–G). Collectively, these observations suggest that astrocyte MyD88 signaling is closely correlated with leptin responsiveness during long-term over-nutrition.

Figures

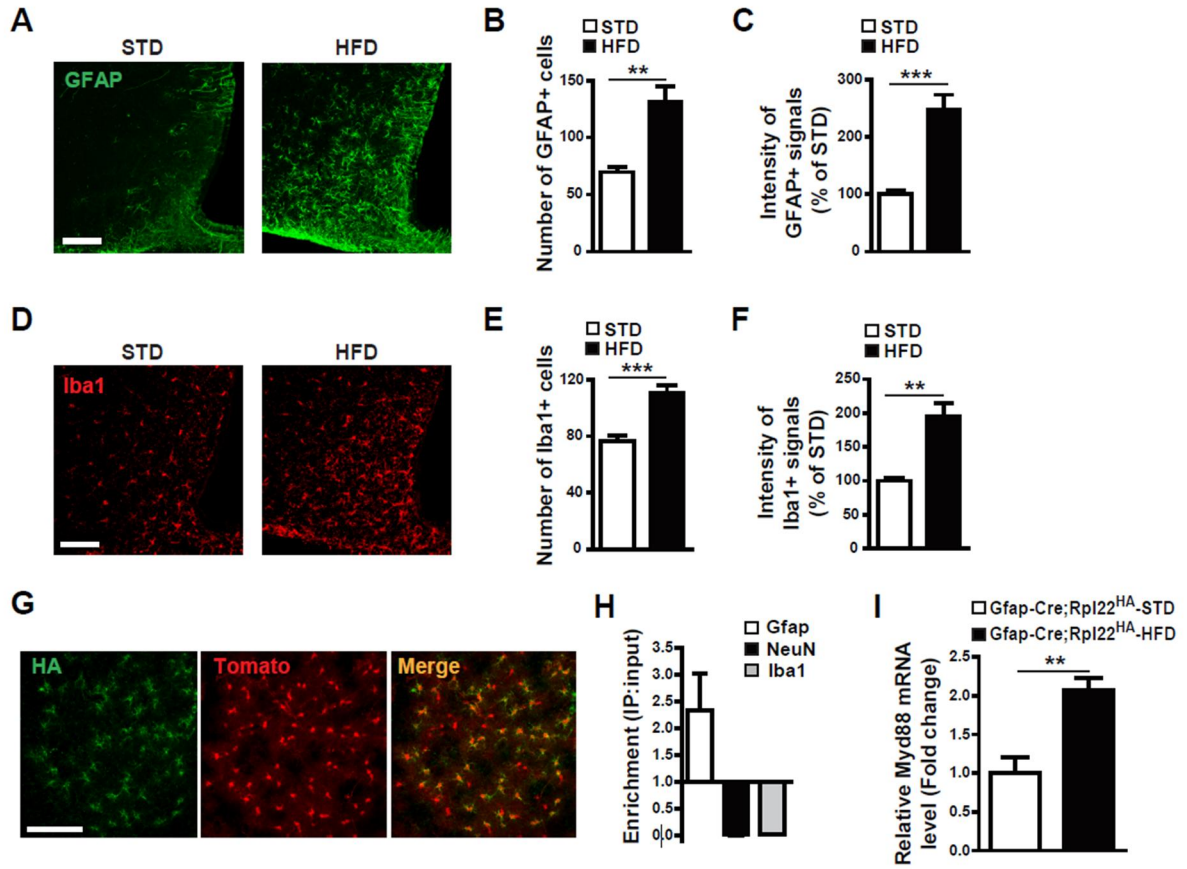

Figure. 1 Increased Myd88 expression during hypothalamic reactive gliosis is induced by eating a high-fat diet (HFD).

(A–F) Immunohistochemical analyses were performed to determine changes in astrocytes and microglia in the hypothalamic arcuate nucleus (ARC) caused by HFD feeding. Representative images (A, D) and calculated data (B, C, E, F) indicate that GFAP-positive astrocytes (A-C) and Iba1-positive microglia (D-F) were increased by an HFD compared with a standard diet (STD) for 16 weeks (n=6-12 sections of 3-6 mice/group). (G–I) Ribo-Tag analyses of *Myd88* mRNA expression in the hypothalamic astrocytes of transgenic mice (*Gfap-Cre;Rpl22*^{HA}) expressing hemagglutinin (HA)-tagged ribosomal protein Rpl22 in GFAP-positive cells. (G) Representative images

showing co-expression of HA and astrocyte-specific tomato signals in the hypothalamic ARC of *Gfap-Cre;Rpl22*^{HA} mice. (H) Real-time PCR data showing enrichment of *Gfap* mRNA (but not NeuN and Iba1 mRNA) in the RNA samples immunoprecipitated with HA antibody compared with the input RNA samples from hypothalamic extracts. (I) Ribo-Tag analyses showing that *Myd88* mRNA expression in the hypothalamic astrocytes of *Gfap-Cre;Rpl22*^{HA} mice was increased by HFD feeding, compared with STD feeding, for 16 leks (n=3–4/group). Data are presented as mean ± SEM. $^{**}p<0.01$, and $^{***}p<0.001$. Scale bar = 100 μm.

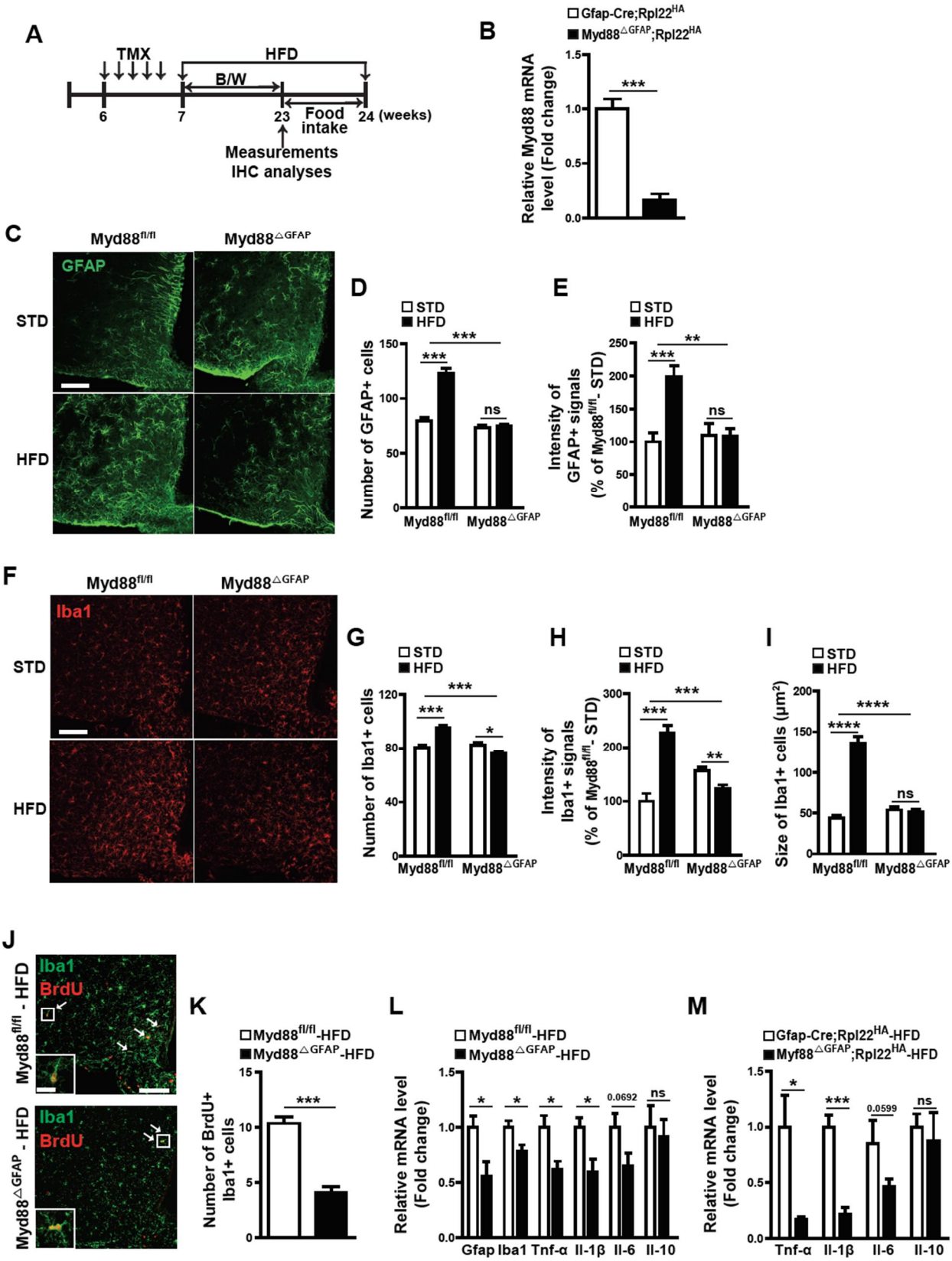
A
TMX
HFD
B/W
6
7
23
Food intake
24 (weeks)
Measurements
IHC analyses
B
Gfap-Cre;Rpl22HA
Myd88△GFAP;Rpl22HA
Relative Myd88 mRNA level (Fold change)
***
C
Myd88fl/fl
Myd88△GFAP
GFAP
STD
HFD
D
STD
HFD
Number of GFAP+ cells
***
ns
Myd88fl/fl
Myd88△GFAP
E
Intensity of GFAP+ signals (% of Myd88fl/fl- STD)
**
F
Iba1
G
Number of Iba1+ cells
*
H
Intensity of Iba1+ signals (% of Myd88fl/fl- STD)
I
Size of Iba1+ cells (μm2)
****
J
Iba1
BrdU
Myd88fl/fl - HFD
Myd88△GFAP - HFD
K
Myd88fl/fl-HFD
Myd88△GFAP-HFD
Number of BrdU+ Iba1+ cells
L
Relative mRNA level (Fold change)
Gfap
Iba1
Tnf-α
Il-1β
Il-6
Il-10
0.0692
ns
M
Gfap-Cre;Rpl22HA-HFD
Myf88△GFAP;Rpl22HA-HFD
0.0599

Figure. 2 HFD-induced hypothalamic reactive gliosis is reduced by astrocyte-specific *Myd88* KO.

(A) Diagram depicts the experimental design. TMX=tamoxifen. B/W=body weight. IHC=immunohistochemistry. (B) The expression of *Myd88* mRNA was determined using a real-time PCR analysis with RNA samples immunoprecipitated with HA antibody from hypothalamic extracts of *Myd88*$^{\triangle GFAP}$;*Rpl22*^{HA} mice that were generated by cross-breeding astrocyte-specific *Myd88* KO mice (*Myd88*$^{\triangle GFAP}$) with transgenic mice (*Rpl22*^{HA}) expressing HA-tagged Rpl22. *Gfap-Cre;Rpl22*^{HA} mice were used as the control (n=4–5/group). (C–I) Control (*Myd88*$^{fl/fl}$) mice and *Myd88*$^{\triangle GFAP}$ mice were fed a STD or HFD for 16 weeks, and their astrocytes and microglia in the hypothalamic ARC were analyzed with immunohistochemistry using GFAP and Iba1 antibodies. Representative images (C, F) and calculated data (D, E, G, H, I) show the effect of astrocyte-specific *Myd88* KO (*Myd88*$^{\triangle GFAP}$) on the HFD-induced increase in the number and intensity of GFAP-positive cells (C–E) and Iba1-positive cells (F-H), and the size of Iba1-positive cells (I) in the ARC compared with the control *Myd88*$^{fl/fl}$ mice (n=3-6 sections of 3–6 mice/group). (J, K) Representative images (J) and calculated data (K) indicate HFD-induced BrdU and Iba1 double-positive cells in the ARC of *Myd88*$^{\triangle GFAP}$ mice and control *Myd88*$^{fl/fl}$ mice after HFD feeding for 8 weeks. White arrows indicate cells double positive for Iba1 and BrdU (n=6 sections of 3 mice/group). (L) Real-time PCR analysis of RNA samples shows the expression of Gfap, Iba1, Tnf-α, Il-1β, Il-6 and Il-10 in the hypothalamus of *Myd88*$^{\triangle GFAP}$ mice and control *Myd88*$^{fl/fl}$ mice after HFD feeding for 16 weeks (n=3/group). (M) Hypothalamic expression of Tnf-α, Il-1β, Il-6 and Il-10 was determined using a real-time PCR analysis of RNA samples (immunoprecipitated with HA antibody) from hypothalamic extracts of

Myd88$^{\triangle GFAP}$;*Rpl22*^{HA} mice and control *Gfap-Cre;Rpl22*^{HA} mice after HFD feeding for 16 weeks (n=3–4/group). Data are presented as mean ± SEM. *p<0.05, **p<0.01, ***p<0.001 and ****p<0.0001. ns, not significant. Scale bar = 100 μm (20 μm for higher magnification view in insets).

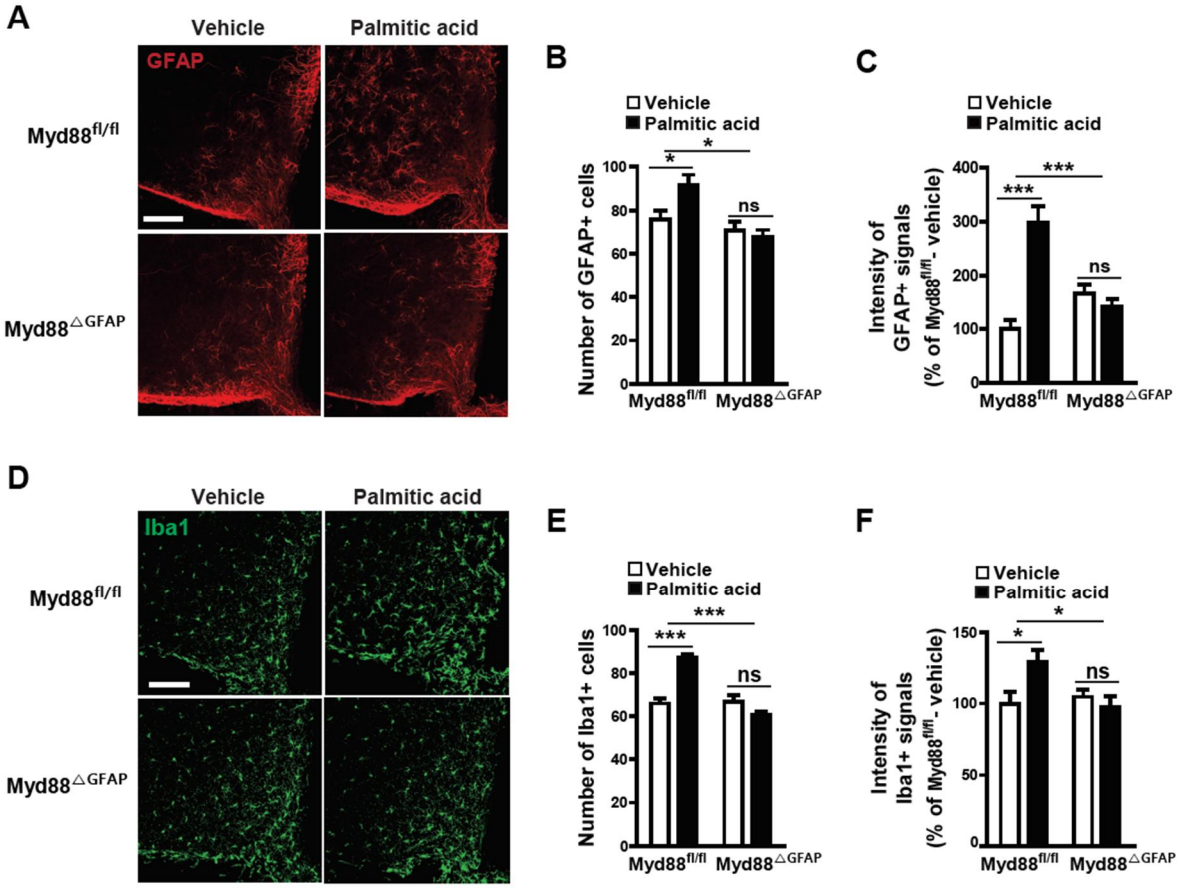

Figure. 3 Palmitic acid–induced hypothalamic gliosis is attenuated by ablation of Myd88 expression in astrocytes.

To identify the effect of astrocyte MyD88 on saturated free fatty acid–induced hypothalamic reactive gliosis, astrocyte-specific *Myd88* KO mice (*Myd88*$^{\triangle GFAP}$) and control *Myd88*$^{fl/fl}$ mice were icv administered palmitic acid (50 pmol/2 μl), and their astrocytes and microglia were immunohistochemically analyzed with GFAP and Iba1 antibodies. (A, D) Representative images show palmitic acid–induced changes in hypothalamic GFAP-positive cells (A) and Iba1-positive cells (D) in *Myd88*$^{fl/fl}$ mice and *Myd88*$^{\triangle GFAP}$ mice. (B, C, E, F) Number and intensity of GFAP-positive cells (B, C) and

Iba1-positive cells (E, F) observed in the hypothalamic ARC of *Myd88*$^{fl/fl}$ mice and *Myd88*$^{\triangle GFAP}$ mice after icv injection of palmitic acid or vehicle (n=4–6 sections of 2–3 mice/group). Data are presented as mean ± SEM. $^{*}p<0.05$ and $^{***}p<0.001$. ns, not significant. Scale bar = 100 µm.

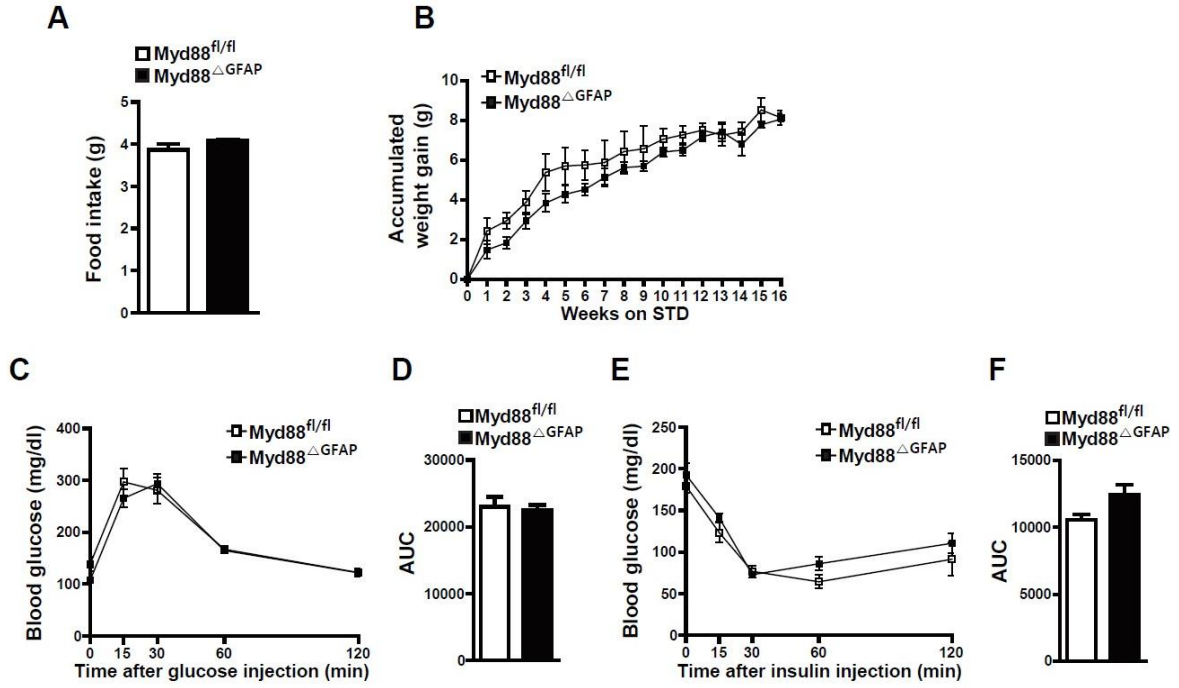

Figure. 4. Astrocyte-specific *Myd88* KO does not change energy metabolism of mice under a standard diet (STD) feeding condition.

Metabolic parameters of astrocyte-specific *Myd88* KO (*Myd88*$^{\triangle GFAP}$) mice and control *Myd88*$^{fl/fl}$ mice were determined after STD feeding for 16 weeks. No difference was observed between the experimental groups in average daily food intake (A), body weight (B), glucose tolerance test (C, D), or insulin tolerance test (E, F) (n=4–5/group). STD=standard food. AUC=area under curve. Data are presented as mean ± SEM.

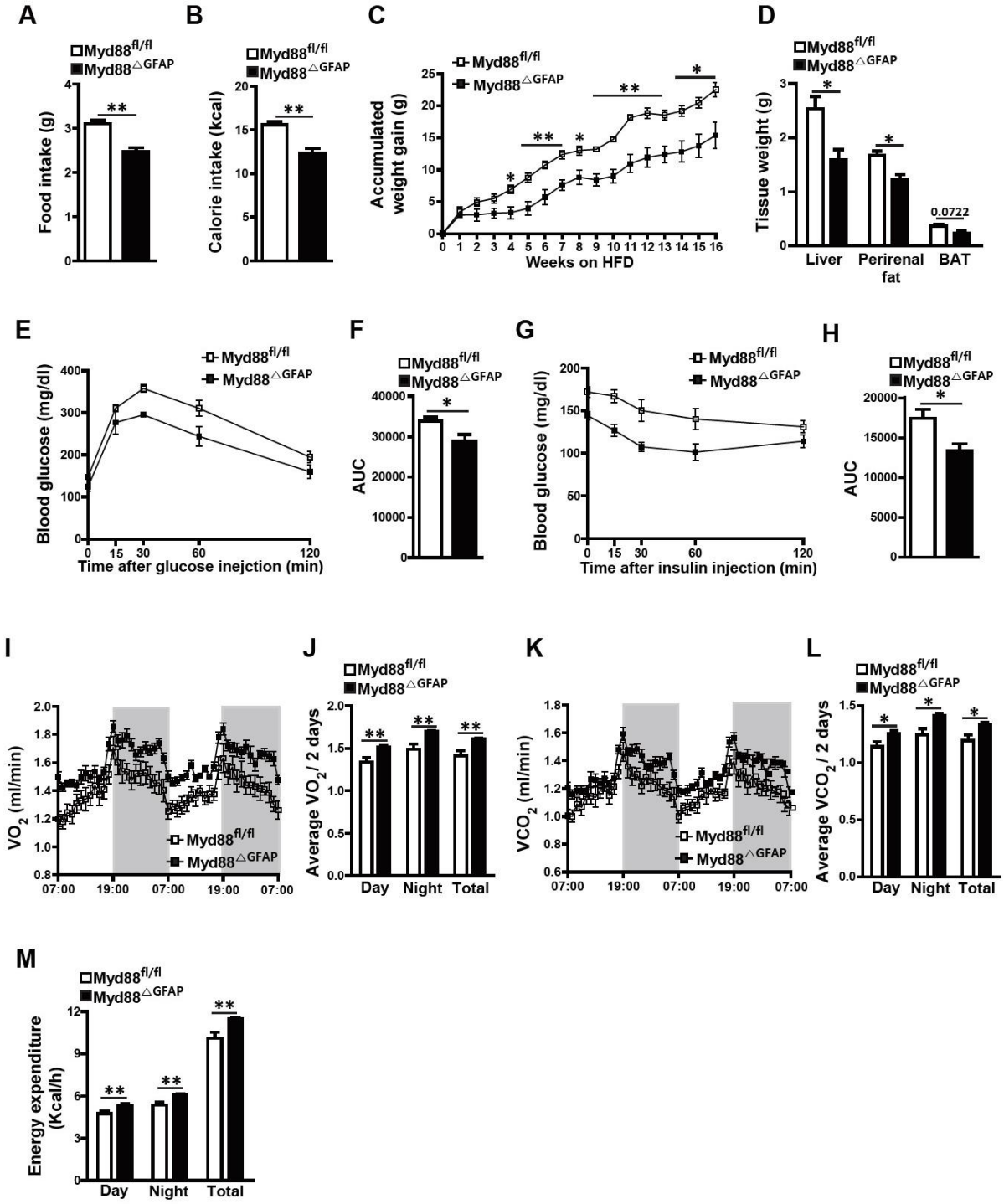
A
B
C
D
Myd88fl/fl
Myd88△GFAP
Food intake (g)
Calorie intake (kcal)
Accumulated weight gain (g)
Weeks on HFD
Tissue weight (g)
Liver
Perirenal fat
BAT
0.0722
E
F
G
H
Blood glucose (mg/dl)
Time after glucose inejction (min)
AUC
Time after insulin injection (min)
I
J
K
L
VO2 (ml/min)
Average VO2/ 2 days
VCO2 (ml/min)
Average VCO2/ 2 days
Day
Night
Total
07:00
19:00
M
Energy expenditure (Kcal/h)

Figure. 5 Astrocyte-specific *Myd88* KO affects HFD-induced obesity.

Astrocyte-specific *Myd88* KO (*Myd88*$^{\triangle GFAP}$) mice and control *Myd88*$^{fl/fl}$ mice were fed an HFD for 16 weeks, and then their metabolic parameters were measured. (A, B) Average daily food intake (A) and average daily calorie intake (B) were measured for a week at 23-24 weeks of age during HFD feeding (n=4/group). (C) The accumulated weight gain of the mice was observed every week during HFD feeding (n=4/group). HFD=High-fat diet. (D) The weight of adipose tissues was measured at 24 weeks of age (n=4/group). BAT=brown adipose tissue. (E-H) Glucose tolerance testing (E, F) and insulin tolerance testing (G, H) were carried out in mice after HFD feeding for 16 weeks (n=5–9/group). AUC=area under curve. (I–M) Indirect calorimetry measurements were performed in metabolic cages to determine changes in the oxygen consumption (VO_2) (I, J), carbon dioxide generation (VCO_2) (K, L), and energy expenditure (M) of mice after HFD feeding for 16 weeks (n=8/group). Data are presented as mean ± SEM. $^{*}p<0.05$, and $^{**}p<0.01$.

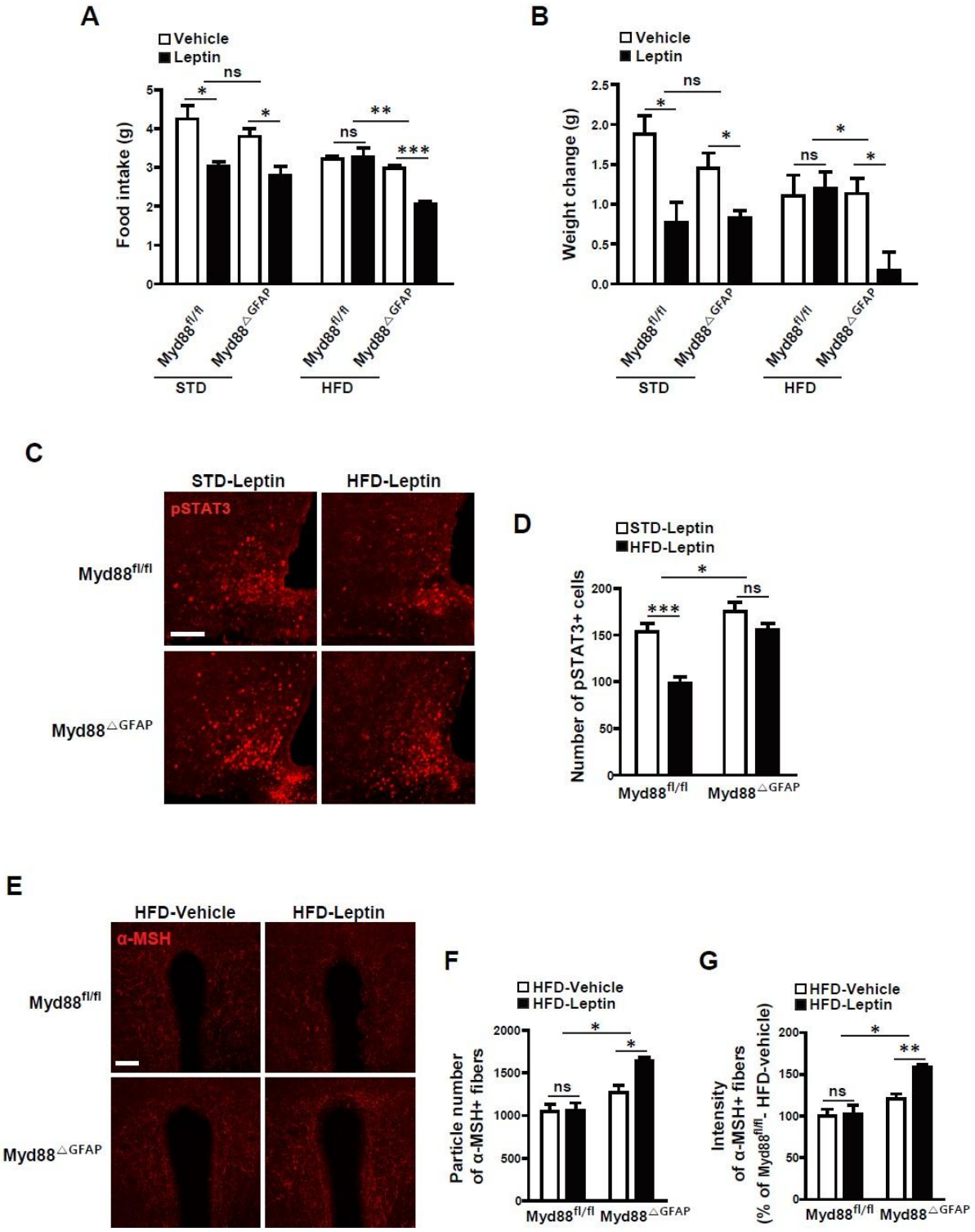
A
Vehicle
Leptin
Food intake (g)
ns
*
*
ns
**
***
Myd88fl/fl
Myd88△GFAP
Myd88fl/fl
Myd88△GFAP
STD
HFD
B
Vehicle
Leptin
Weight change (g)
ns
*
*
ns
*
*
Myd88fl/fl
Myd88△GFAP
Myd88fl/fl
Myd88△GFAP
STD
HFD
C
STD-Leptin
HFD-Leptin
pSTAT3
Myd88fl/fl
Myd88△GFAP
D
STD-Leptin
HFD-Leptin
Number of pSTAT3+ cells
*
***
ns
Myd88fl/fl
Myd88△GFAP
E
HFD-Vehicle
HFD-Leptin
α-MSH
Myd88fl/fl
Myd88△GFAP
F
HFD-Vehicle
HFD-Leptin
Particle number of α-MSH+ fibers
*
*
ns
Myd88fl/fl
Myd88△GFAP
G
HFD-Vehicle
HFD-Leptin
Intensity of α-MSH+ fibers (% of Myd88fl/fl- HFD-vehicle)
*
**
ns
Myd88fl/fl
Myd88△GFAP

Figure. 6 Astrocyte-specific *Myd88* KO enhances leptin responsiveness after long-term HFD feeding.

(A, B) To identify the effects of astrocyte-specific *Myd88* KO (*Myd88*$^{\triangle GFAP}$) on HFD-induced leptin resistance, mice were fed an HFD for 16 weeks, and their food intake (A) and body weight (B) were measured for 24 h after an intraperitoneal injection of leptin (2 mg/kg) or vehicle (n=3–4/group). (C, D) Representative immunohistochemical images (C) and calculated graphs (D) show that leptin-induced pSTAT3 in the arcuate nucleus had deteriorated in the control *Myd88*$^{fl/fl}$ mice after 16 leks of HFD feeding. However, the *Myd88*$^{\triangle GFAP}$ mice fed the HFD for 16 weeks showed a leptin-induced pSTAT3 level similar to those with STD feeding. (E–G) Representative images (E) and calculated data (F, G) reveal that leptin induced an increase in α-MSH immuno-positive signals in the paraventricular nucleus of the *Myd88*$^{\triangle GFAP}$ mice but not the control *Myd88*$^{fl/fl}$ mice after 16 weeks of HFD feeding. (n=3 sections of 3 mice/group). Data are presented as mean ± SEM. $^{*}p<0.05$, $^{**}p<0.01$ and $^{***}p<0.001$. ns=not significant. Scale bar = 100 μm.

Discussion

In the present study, I found that *Myd88* expression in hypothalamic astrocytes was increased by long-term HFD feeding and that astrocyte-specific ablation of *Myd88* ameliorated the obesity-related metabolic phenotype induced by HFD consumption. The current observations demonstrate that MyD88 signaling in astrocytes is a critical contributor to the hypothalamic inflammation–induced pathogenesis of obesity.

In this study, I focused on the role of MyD88 signaling in astrocytes as a mediator of hypothalamic inflammation during HFD feeding. Interestingly, I found that HFD-induced reactive gliosis was decreased in hypothalamic ARC of mutant mice lacking *Myd88* expression in astrocytes compared to control mice. Moreover, a direct icv infusion of sFFAs induced reactive gliosis in hypothalamic ARC of control mice, but not in astrocyte-specific *Myd88* KO mice. These results suggested that MyD88 signaling in astrocytes plays a critical role in the hypothalamic reactive gliosis induced by HFD and sFFAs. In animals chronically fed an HFD, reactive astrocytes in the hypothalamus induced neuronal damage by secreting proinflammatory cytokines [14, 26]. In this DIO model, the proinflammatory cytokines released by hypothalamic astrocytes and microglia activated cytokine receptors on the hypothalamic proopiomelanocortin (POMC) and agouti-related peptide (AgRP) neurons [12, 20, 30, 31]. In the current study, astrocyte-specific *Myd88* KO resulted in a decrease in activation of microglia in the ARC and expression of proinflammatory cytokines in the hypothalamus during HFD feeding. These changes might be due to that astrocyte-specific deletion of *Myd88* gene caused a decrease in HFD-induced intracellular signaling for the activation of proinflammatory cytokine expression in the hypothalamic

astrocytes. Since the ARC of the hypothalamus is considered as a major site for the actions of POMC and AgRP neurons that dynamically participate in the central control of energy homeostasis, I focused on the action of astrocytes in the hypothalamic ARC. However, I could not exclude a possible contribution of astrocytes in other sites of hypothalamus including the median eminence and third ventricular linings to the development of inflammatory processes. Therefore, further studies are required to identify subpopulations of hypothalamic astrocytes that are important in the initiation of hypothalamic inflammation during a long-term exposure to over-nutrition.

HFD-induced hypothalamic reactive gliosis and inflammatory responses are important factors in leptin sensitivity during HFD consumption [14, 20]. Despite high circulating leptin levels, over-nutrition-induced obese mice show a reduced responsiveness to the appetite- and weight gain–suppressing effects of leptin, which is generally called *leptin resistance* and is a critical element in the development of obesity. It has been proposed that development of leptin resistance is coupled to multiple cellular events including abnormalities of leptin signaling, leptin transportation, and leptin receptor trafficking [32]. Particularly, it is currently accepted that the hypothalamic gliosis accompanied by enhanced inflammation responses is regarded as a crucial pathological element during the over-nutrition period [12, 14, 20]. In line with these notions, I observed that the *Myd88*$^{\Delta GFAP}$ mice displayed anti-obesity phenotype in association with improved responsiveness to leptin after long-term HFD feeding. In accordance with the behavioral observations, I confirmed the leptin-triggered induction of pSTAT3, a general molecular marker for the leptin responsiveness, in the hypothalamic ARC. Given that leptin signaling operates the activity of POMC neurons that govern hypothalamic cells expressing melanocortin

receptors by releasing α-MSH, I further validated improved responsiveness of the *Myd88* KO mice to leptin by identifying the enhanced innervation of α-MSH in the hypothalamic PVN, even after long-term HFD feeding. These observations strengthen the underappreciated role of astrocytic TLR-MyD88 signaling in the regulation of over-nutrition-induced hypothalamic inflammation and metabolic abnormalities. Notably, previous literatures have suggested that leptin receptors are present in hypothalamic astrocytes and participate in the central control of energy metabolism [33-35]. However, active role of the leptin receptors in hypothalamic astrocytes is still controversial. Thus, this study raised an important question whether MyD88 is connected to the leptin receptor signaling in hypothalamic astrocytes. It is well-known that over-nutrition-induced inflammatory factors activate NF-κB signaling, which up-regulates negative regulators of leptin signaling, such as suppressor of cytokine signaling 3, and thus inhibits pSTAT3 signaling [20, 36, 37]. In addition, elevated activity of TLRs and MyD88 coupling leads to the activation of NF-κB signaling in hypothalamic neurons [20, 21]. Therefore, these evidences and current findings together suggest that MyD88 signaling in astrocytes is important in leptin resistance caused by HFD-induced inflammation and obesity pathogenesis.

Although studies to understand the mechanisms that underlie leptin resistance during HFD consumption have focused on the role of astrocytes and microglia, the cooperative actions and relationships between them during HFD-induced neuroinflammation remain largely unknown. Several reports have revealed that crosstalk occurs between astrocytes and microglia through the release of signaling factors (such as cytokines and chemokines) that contribute to the pathogenesis of neuroinflammation and neurodegeneration [31, 38]. A recent *in vitro* study showed that

the accumulation of lipid droplets in hypothalamic astrocytes could be induced by sFFA treatment and led to the activation of microglia through inflammatory cytokines [39]. In this study, astrocyte-specific *Myd88* KO blocked HFD-induced microglial activation. In line with previous reports, this result might indicate that astrocyte-specific *Myd88* KO decreased HFD-induced expression of cytokines in astrocytes, which further indicates crosstalk between astrocytes and microglia and the importance of astrocyte MyD88 signaling in HFD-induced obesity.

In summary, present study reports that MyD88 signaling in astrocytes is a key mediator of obesity pathogenesis and highlights its contribution to over-nutrition-induced reactive gliosis and leptin resistance in the hypothalamus. These observations suggest that MyD88 signaling in hypothalamic astrocytes could be an important novel target for the treatment of metabolic disorders such as leptin resistance and obesity.

References

1. Malik VS, Willett WC, Hu FB: Global obesity: trends, risk factors and policy implications. Nat Rev Endocrinol. 2013;9:13-27.

2. Bluher M: Obesity: global epidemiology and pathogenesis. Nat Rev Endocrinol. 2019;15:288-298.

3. Thaler JP, Guyenet SJ, Dorfman MD, Wisse BE, Schwartz MW: Hypothalamic inflammation: marker or mechanism of obesity pathogenesis? Diabetes. 2013;62:2629-2634.

4. Dietrich MO, Horvath TL: Hypothalamic control of energy balance: insights into the role of synaptic plasticity. Trends Neurosci. 2013;36:65-73.

5. Horvath TL: Synaptic plasticity in energy balance regulation. Obesity. 2006;14 Suppl 5:228S-233S.

6. Lam TK, Schwartz GJ, Rossetti L: Hypothalamic sensing of fatty acids. Nat Neurosci. 2005;8:579-584.

7. Waterson MJ, Horvath TL: Neuronal Regulation of Energy Homeostasis: Beyond the Hypothalamus and Feeding. Cell Metab. 2015;22:962-970.

8. Williams KW, Elmquist JK: From neuroanatomy to behavior: central integration of peripheral signals regulating feeding behavior. Nat Neurosci. 2012;15:1350-1355.

9. Belanger M, Allaman I, Magistretti PJ: Brain energy metabolism: focus on astrocyte-neuron metabolic cooperation. Cell Metab. 2011;14:724-738.

10. Clarke LE, Barres BA: Emerging roles of astrocytes in neural circuit development. Nat Rev Neurosci. 2013;14:311-321.

11. Kalin S, Heppner FL, Bechmann I, Prinz M, Tschop MH, Yi CX: Hypothalamic innate immune reaction in obesity. Nat Rev Endocrinol. 2015;11:339-351.

12. Thaler JP, Yi CX, Schur EA, Guyenet SJ, Hwang BH, Dietrich MO, Zhao X, Sarruf DA, Izgur V, Maravilla KR, et al: Obesity is associated with hypothalamic injury in rodents and humans. J Clin Invest. 2012;122:153-162.

13. Buckman LB, Thompson MM, Moreno HN, Ellacott KL: Regional astrogliosis in the mouse hypothalamus in response to obesity. J Comp Neurol. 2013;521:1322-1333.

14. Garcia-Caceres C, Yi CX, Tschop MH: Hypothalamic astrocytes in obesity. Endocrinol Metab Clin North Am. 2013;42:57-66.

15. Argente-Arizon P, Frewere-Regatillo A, Argente J, Choln JA: Role of non-neuronal cells in body weight and appetite control. Front Endocrinol. 2015;6:42.

16. Shi H, Kokoeva MV, Inouye K, Tzameli I, Yin H, Flier JS: TLR4 links innate immunity and fatty acid-induced insulin resistance. J Clin Invest. 2006;116:3015-3025.

17. O'Neill LA, Golenbock D, Bowie AG: The history of Toll-like receptors - redefining innate immunity. Nat Rev Immunol. 2013;13:453-460.

18. Konner AC, Bruning JC: Toll-like receptors: linking inflammation to metabolism. Trends Endocrinol Metab. 2011;22:16-23.

19. Santamarina AB, Jamar G, Mennitti LV, de Rosso VV, Cesar HC, Oyama LM, Pisani LP: The Use of Jucara (Euterpe edulis Mart.) Supplementation for Suppression of NF-kappaB Pathway in the Hypothalamus after High-Fat Diet in Wistar Rats. Molecules. 2018;23.

20. de Git KC, Adan RA: Leptin resistance in diet-induced obesity: the role of

hypothalamic inflammation. Obes Rev. 2015;16:207-224.

21. Kleinridders A, Schenten D, Konner AC, Belgardt BF, Mauer J, Okamura T, Wunderlich FT, Medzhitov R, Bruning JC: MyD88 signaling in the CNS is required for development of fatty acid-induced leptin resistance and diet-induced obesity. Cell Metab. 2009;10:249-259.

22. Sanz E, Yang L, Su T, Morris DR, McKnight GS, Amieux PS: Cell-type-specific isolation of ribosome-associated mRNA from complex tissues. Proc Natl Acad Sci U S A. 2009;106:13939-13944.

23. Kang SS, Ebbert MTW, Baker KE, Cook C, Wang X, Sens JP, Kocher JP, Petrucelli L, Fryer JD: Microglial translational profiling reveals a convergent APOE pathway from aging, amyloid, and tau. J Exp Med. 2018;215:2235-2245.

24. Kim JD, Yoon NA, Jin S, Diano S: Microglial UCP2 Mediates Inflammation and Obesity Induced by High-Fat Feeding. *Cell Metab* 2019;30:952-962.

25. Livak KJ, Schmittgen TD: Analysis of relative gene expression data using real-time quantitative PCR and the 2(-Delta Delta C(T)) Method. Methods. 2001;25:402-408.

26. Garcia-Caceres C, Fuente-Martin E, Argente J, Choln JA: Emerging role of glial cells in the control of body weight. Mol Metab. 2012;1:37-46.

27. Jin S, Kim JG, Park JW, Koch M, Horvath TL, Lee BJ: Hypothalamic TLR2 triggers sickness behavior via a microglia-neuronal axis. Sci Rep. 2016;6:29424.

28. Valdearcos M, Robblee MM, Benjamin DI, Nomura DK, Xu AW, Koliwad SK: Microglia dictate the impact of saturated fat consumption on hypothalamic inflammation and neuronal function. Cell Rep. 2014;9:2124-2138.

29. Gupta S, Knight AG, Gupta S, Keller JN, Bruce-Keller AJ: Saturated long-chain fatty acids activate inflammatory signaling in astrocytes. J Neurochem. 2012;120:1060-1071.

30. Horvath TL, Sarman B, Garcia-Caceres C, Enriori PJ, Sotonyi P, Shanabrough M, Borok E, Argente J, Choln JA, Perez-Tilve D, et al: Synaptic input organization of the melanocortin system predicts diet-induced hypothalamic reactive gliosis and obesity. Proc Natl Acad Sci U S A. 2010;107:14875-14880.

31. Rahman MH, Kim MS, Lee IK, Yu R, Suk K: Interglial Crosstalk in Obesity-Induced Hypothalamic Inflammation. Front Neurosci. 2018;12:939.

32. Morris DL, Rui L: Recent advances in understanding leptin signaling and leptin resistance. Am J Physiol Endocrinol Metab. 2009;297:E1247-1259.

33. Valdearcos M, Myers MG, Koliwad SK: Hypothalamic microglia as potential regulators of metabolic physiology. *Nat Metab* 2019;7:731-742.

34. Tsunekawa T, Banno R, Mizoguchi A, Sugiyama M, Tominaga T, Onoue T, Hagiwara D, Ito Y, Iwama S, Goto M, et al: Deficiency of PTP1B Attenuates Hypothalamic Inflammation via Activation of the JAK2-STAT3 Pathway in Microglia. *EBioMedicine* 2017, 16:172-183.

35. Kim JG, Suyama S, Koch M, Jin S, Argente-Arizon P, Argente J, Liu ZW, Zimmer MR, Jeong JK, Szigeti-Buck K, et al: Leptin signaling in astrocytes regulates hypothalamic neuronal circuits and feeding. *Nat Neurosci* 2014;17:908-910.

36. Jang PG, Namkoong C, Kang GM, Hur MW, Kim SW, Kim GH, Kang Y, Jeon MJ, Kim EH, Lee MS, et al: NF-kappaB activation in hypothalamic pro-opiomelanocortin neurons is essential in illness- and leptin-induced anorexia.

J Biol Chem. 2010;285:9706-9715.

37. Shi X, Wang X, Li Q, Su M, Chew E, Wong ET, Lacza Z, Radda GK, Tergaonkar V, Han W: Nuclear factor kappaB (NF-kappaB) suppresses food intake and energy expenditure in mice by directly activating the Pomc promoter. Diabetologia. 2013;56:925-936.

38. Jha MK, Jo M, Kim JH, Suk K: Microglia-Astrocyte Crosstalk: An Intimate Molecular Conversation. Neuroscientist. 2019;25:227-240.

39. Kwon YH, Kim J, Kim CS, Tu TH, Kim MS, Suk K, Kim DH, Lee BJ, Choi HS, Park T, et al: Hypothalamic lipid-laden astrocytes induce microglia migration and activation. FEBS Lett. 2017;591:1742-1751.

CHAPTER 2

Phosphorylated eIF2α regulates AgRP neuronal activity

Abstract

Regulation of protein synthesis is a rapid and effective means to respond to changes in the cellular environment. A central mechanism for protein synthesis involves phosphorylation of eukaryotic translation initiation factor 2α (eIF2α), which reduces protein synthesis and is associated with various cellular stresses such as endoplasmic reticulum (ER) stress. However, the function of eIF2α signaling in the hypothalamus that controls whole-body energy metabolism is largely unknown. Here, I demonstrate the role of eIF2α phosphorylation in hypothalamic AgRP neurons in the regulation of feeding and energy balance. The neuronal activity in hypothalamic arcuate nucleus and feeding behavior were significantly attenuated in AgRP neuron-specific eIF2α phosphorylation deficient mice (*AgRP*$^{eIF2\alpha A/A}$ mice). Also, *AgRP*$^{eIF2\alpha A/A}$ mice displayed a greater increase in energy expenditure and stronger sensitivity to leptin than control mice. Intriguingly, I further identified that the deficiency of eIF2α phosphorylation in AgRP neurons decreased the ER stress-induced unfolded protein response (UPR) signaling as well as the expression of genes for autophagy and mitochondrial dynamics in the AgRP neurons after overnight fasting. Collectively, these findings suggest that eIF2α signaling in hypothalamic AgRP neurons as an energy sensor controls activation of AgRP neurons through regulation of the UPR signaling and cellular responses in AgRP neurons, and affects the feeding behavior and whole-body energy balance.

Introduction

The maintenance of energy balance in the whole-body is one of the main issues in modern societies. Therefore, the regulation of appetite is focused due to its importance for maintaining energy balance, which is determined by calorie intake and energy expenditure [1-3]. In particular, the agouti-related peptide (AgRP) neurons in the arcuate nucleus (ARC) of hypothalamus are indispensable for feeding behavior and energy metabolism. Previous studies showed that the over-expression of AgRP result in obesity, and genetic ablation of AgRP neuron in mice lead to anorexia and death within a few days [4-6]. The hypothalamic AgRP neurons sense the energy deficit through responding to metabolic hormones such as ghrelin and insulin [7, 8]. Accordingly, the dysfunction of AgRP neurons leads to energy imbalance and metabolic diseases [9, 10].

According to recent literatures, cellular responses such as autophagy and mitochondrial dynamics in the AgRP neurons influence the whole-body energy metabolism through the activation of AgRP neurons during energy deprivation. The increased free fatty acids (FFAs) by fasting condition induced autophagy in hypothalamic AgRP neurons and then affected the feeding through activation of AgRP neurons [11, 12]. Furthermore, food deprivation leads to a decrease in mitochondria size in AgRP neurons, which is characteristic of changes in mitochondrial dynamics towards fission [13, 14]. However, most of the other intracellular responses to systemic metabolic challenges in the hypothalamic AgRP neurons during energy deprivation remain unexplored.

Eukaryotic translation initiation factor 2 α (eIF2α) is a subunit of the eIF2 complex

(α, β and γ), which plays a critical role in the control of translation initiation upon diverse cellular responses. During the initiation of translation, eIF2 recruits the initiator methionyl-tRNA (Met-tRNAi) and GTP to form the ternary complex that then bind to the ribosome. In mammals, α subunit of eIF2 at Ser 51 is phosphorylated by different four kinases, protein kinase R (PKR)-like endoplasmic reticulum kinase (PERK), general control nonderepressible 2 (GCN2), RNA-activated protein kinase (PKR) and heme-regulated inhibitor kinase (HRI) in response to diverse cellular stress including endoplasmic reticulum (ER) stress, amino acid deficiency, viral infection and heme deficiency [15, 16]. ER stress activates a complex intracellular signaling pathway called the unfolded protein response (UPR), which inhibits global protein synthesis and enhances the capacity of productive folding and degradation mechanisms through transcription of genes encoding ER chaperones and ER-associated degradation (ERAD) [17, 18]. The eIF2α phosphorylation is not only responsible for attenuation of global translation initiation, but also enhances the adaptive gene expression to restore cellular homeostasis such as activating transcription factor 4 (ATF4) and C/EBP-homologous protein (CHOP). Furthermore, eIF2α phosphorylation is also required during ER stress for activation of activating transcription factor 6 α (ATF6α) and induction of spliced X-box binding protein 1 (XBP1) [19-21]. Thus, eIF2α phosphorylation is responsible for transcriptional and translational reprogramming to protect the stressed cells during cellular stress.

Recently, it has been proposed that eIF2α phosphorylation in pancreatic beta cells and hepatocytes plays an important role in the physiological processes during stress responses such as oxidative damage and high-fructose diet [22, 23]. Moreover, the induction of eIF2α signaling in the hypothalamus affects the food intake during amino

acid deprivation [24]. In addition, several studies have demonstrated that ER stress plays an important role in obesity-induced insulin resistance and type 2 diabetes [25-27]. Furthermore, ER stress-induced eIF2α phosphorylation attenuated the hypothalamic POMC processing during overnutrition and thus caused obesity [28]. Taken together, eIF2α is affected by energy excess-induced ER stress. Thus, these evidences raised an important questions whether hypothalamic eIF2α is influenced by energy status and regulates neuronal activity which control energy balance. However, it is unclear whether the ER stress-induced UPR signaling pathway and eIF2α signaling in the hypothalamic AgRP neurons are triggered by energy deprivation and thus linked to the feeding behavior through regulation of AgRP neurons activity. In this study, I investigated whether eIF2α phosphorylation in AgRP neurons is involved in food deprivation-induced UPR signaling pathway in the hypothalamic AgRP neurons and whether altering the feeding behavior and energy balance through activation of AgRP neurons.

Materials and Methods

Animals

Animals were fed a standard diet (STD, Feedlab, Gyeonggi-Do, Korea) *ad libitum* and given free access to tap water. All animals were maintained in temperature- and humidity-controlled rooms with a 12 h/12 h light-dark cycle, with the lights on from 7:00 a.m. to 7:00 p.m.

The mice with homozygous *eIF2α Ser51/Ala* (herein, *A/A*) mutation where Ser51 of eIF2α is changed to Ala have impaired phosphorylation of eIF2α. However, mutant mice have lethality phenotype. To prevent the lethality of homozygous *eIF2α A/A* mice, mice received the wild-type (WT) eIF2α from a *loxP*-flanked (floxed) WT *eIF2α* transgene (*fTg*) [23]. To elucidate the role of eIF2α phosphorylation in the hypothalamic AgRP neurons, *A/A* mutant mice bearing floxed WT *eIF2α* transgene (*A/A;fTg/Tg* mice) were crossbred with *AgRP-Cre* mice (Stock No. 012899, Jackson Laboratory, Bar Harbor, ME, USA) to generate phosphorylation of eIF2α deficient mice specifically in the AgRP neurons (*AgRP*$^{eIF2\alpha A/A}$ mice). The transgene was designed to coordinately induce enhanced green fluorescence protein (EGFP) expression upon Cre recombinase-mediated deletion of the *eIF2α*-cording region (Figure 2A). As controls, homozygous *A/A* mice carrying a single-copy transgene (*A/A;fTg/0* mice). *Rosa26-lox-stop-lox-tdTomato* mice (Ai14 reporter mice) were crossbred with *AgRP-Cre* mice or *AgRP*$^{eIF2\alpha A/A}$ mice to label all AgRP-expressing cells with tomato signals (*AgRP-Cre;Ai14* mice or *AgRP*$^{eIF2\alpha A/A}$*;Ai14* mice). Transgenic mice expressing human *Renilla* green fluorescence protein (hrGFP) in NPY neurons (*NPY-hrGFP* mice, Stock No. 006417, Jackson Laboratory) was used for immunohistochemical analysis. All

animals and procedures used were in accordance with the guidelines and approval of the Institutional Animal Care and Use Committee at the university of Ulsan (permit number: BJL-17-040).

Ribo-Tag system

To analyze mRNA species that are specifically translated in hypothalamic AgRP and POMC neurons, I used the Ribo-Tag translational profiling system [29, 30]. In this study, I used *Rpl22*^{HA} mice (Stock No. 011029, Jackson Laboratory), which have a *loxP*-flanked wild-type exon 4 followed by an identical exon 4 tagged with hemagglutinin (HA), as the Ribo-Tag animal. Crossbreeding Ribo-Tag mice with mice expressing Cre recombinase resulted in the deletion and replacement of the floxed wild-type exon 4 with the HA-tagged exon 4 in cells expressing Cre. The *AgRP*$^{eIF2\alpha A/A}$ mice were crossbred with *Rpl22*^{HA} mice to generate *AgRP*$^{eIF2\alpha A/A}$;*Rpl22*^{HA} mice that had both HA-tagged ribosomal protein Rpl22 and eIF2α phosphorylation deficiency in AgRP neurons. The *Rpl22*^{HA} mice were also crossed with *AgRP-Cre* mice, which resulted in control mice bearing an AgRP neuron-specific Ribo-Tag system (*AgRP-Cre;Rpl22*^{HA} mice). To analyzed mRNA in POMC neurons, *POMC-Cre* mice (Stock No. 005965, Jackson Laboratory) were crossed with *Rpl22*^{HA} mice (*POMC-Cre;Rpl22*^{HA} mice).

RNA isolation with the Ribo-Tag system was conducted as previously described [29, 30]. Briefly, dissected hypothalamus samples were collected from animals and homogenized. RNA was extracted from 10% of the cleared lysate and used as input. The remaining lysate was incubated with mouse anti-HA antibody for 4 h at 4°C followed by the addition of protein G agarose beads (LGP-1018B, Lugen, Gyeonggi-Do, Korea) and overnight incubation at 4°C. The beads were washed three times in high salt

solution. The bound ribosomes and RNA were separated from the beads with 30 sec of vortexing, and RNA was further purified using a QIAGEN RNeasy Micro Kit (74034, Qiagen, Hilden, Germany). After RNA isolation, I obtained 10–20 ng of RNA sample/hypothalamus. The RNA samples were then subjected to real-time PCR analysis.

Measurement of food intake and ISRIB administration

Five days before I began the food intake measurements, I moved the mice into individual cages and allowed them to acclimatize to their new environment. Food intake was measured for a week at 16-17 weeks of age during STD feeding and calculated as an average daily food intake. Average of meal size and duration and meal number for 12 h after overnight fasting were measured using an indirect calorimetry system (Promethion, Sable Systems, Las Vegas, NV, USA). Data acquisition and instrument control were coordinated by MetaScreen software (version 2.3.12), and the obtained raw data were processed using ExpeData (version 1.9.14, Sable Systems). Body weight was measured every week during STD feeding. To determine how integrated stress response inhibitor (ISRIB, SML0843, Sigma-Aldrich, St. Louis, MO, USA), which blocks phosphorylated eIF2α signaling, affected feeding behavior, mice were intraperitoneally (i.p.) injected with vehicle (DMSO) or ISRIB (2.5 mg/kg) 90 min before refeeding after overnight fasting. The food intake of the individually caged animals was monitored for 1 h and 4 h after overnight fasting.

Cannulation and administration of leptin, ghrelin and salubrinal

For intracerebroventricular (icv) cannula implantation, mice were anesthetized by ip

injection of tribromoethanol (250 mg/kg, Sigma-Aldrich) and placed in a stereotaxic apparatus (Stoelting, Wood Dale, IL, USA). The cannula (26 gauge) was implanted into the right lateral ventricle (1.0 mm lateral, 0.3 mm posterior, and 2.4 mm ventral to the bregma) according to the *Stereotaxic Mouse Brain Atlas* (Paxinos G and Franklin KBJ, 2001, Academic Press, San Diego, CA, USA) and secured to the skull with dental cement. After 7 days of recovery, mice were injected with vehicle (saline) or with recombinant mouse leptin (1 μg/2 μl, R&D Systems, Minneapolis, MN, USA) after overnight fasting. The food intake of the individually caged animals was monitored for 24 h after the injection. For immunohistochemistry analysis, mice were sacrificed 1 h after the injection of leptin. To identify the sensitivity of ghrelin, mice were ip injected with vehicle (saline) or ghrelin (2 μg/2 μl, R&D Systems). The food intake was measured for 1 h and 2 h after injection. To determine effect of salubrinal on feeding, mice were injected with vehicle (DMSO) and salubrinal (2.5 mM/2.5 μl, Sigma-Aldrich). The food intake of the individually caged animals was monitored for 1 h and 4 h after injection.

Immunohistochemistry (IHC)

Animals were deeply anesthetized with tribromoethanol and transcardially perfused with phosphate buffer (PB, 0.1 M, pH 7.4), followed by a fresh fixative of 4% paraformaldehyde in PB. Brains were post-fixed overnight at 4°C, sliced to a thickness of 50 μm using a vibratome (VT1000P; Leica Microsystems, wetzlar, Germany), and then washed several times in PB. Coronal brain sections containing the hypothalamic arcuate nucleus (ARC) were preincubated with 0.2% Triton X-100 (T8787, Sigma-Aldrich) in PB for 30 min to permeabilize the tissues and cells. After further washing with PB, the sections were incubated overnight at room temperature (RT) with rabbit

anti-p-eIF2α antibody (1:1,000; ab32157, Abcam, Cambridge, MA, USA), rabbit anti-pSTAT3 antibody (1:1,000; 9145, Cell Signaling Technology, Beverly, MA, USA), rabbit anti-c-Fos antibody (1:1000; SC-52, Santacuz, California, CA, USA) and mouse anti-HA antibody (1:1,000; MMS-101R, BioLegend, San Diego, CA, USA), rabbit anti-AgRP (1:1000, H-003-57, Phoenix, Burlingame, CA, USA) or at 4°C with sheep anti-α-melanocyte stimulating hormone (MSH) antibody (1:10,000; AB5087, Millipore, Billerica, MA, USA). On the next day, sections were washed in PB. For immunofluorescence staining, sections were incubated with the following secondary antibodies for 2 h at room temperature: goat anti-rabbit Alexa Fluor 488 (1:500; A11008, Invitrogen, Carlsbad, CA, USA), goat anti-rabbit Alexa Fluor 594 (1:500; A11012, Invitrogen), goat anti-mouse Alexa Fluor 647 (1:500; A28181, Invitrogen), goat anti-mouse Alexa Fluor 488 (1:500; A11001, Invitrogen), and donkey anti-sheep Alexa Fluor 594 (1:500; A11016, Invitrogen). Stained brain sections were imaged using an FV-1200 confocal laser-scanning microscope (Olympus America, Inc., Center Valley, PA, USA).

Number of immune-positive cells in the hypothalamic ARC was counted by an unbiased observer. The fiber intensity and particle number of immuno-positive AgRP and α-MSH signals in PVN Were measured using the ImageJ v 1.50 software (National Institutes of Health, Bethesda, MD).

Western blotting

Tissue samples from hypothalamus in the mice were homogenized in T-PER lysis buffer (Pierce Chemical Co., Rockford, IL). Lysis buffer was contained a protease inhibitor cocktail (Roche, Molecular Diagnostics, Mannheim, Germany) and

phosphatase inhibitor cocktail (Roche). Extracted proteins (10-30 μg) were separated by 10% sodium dodecyl sulfate-polyacrylamide gel electrophoresis and transferred to polyvinylidene fluoride membrane (Millipore Corp). The membrane was blocked in blocking buffer and incubated overnight at 4°C with antibodies specific to p-eIF2α (1:1,000; ab32157, Abcam) and eIF2α (1:1000, 5324, Cell Signaling Technology). Blots were then incubated with horseradish peroxidase-conjugated anti-rabbit (1:4000, sc-2004, Santa Cruz) for 1 h at room temperature. Immunoreactivity was detected with an enhanced chemiluminescence (ECL) kit (Amersham Pharmacia Biotech., Buckinghamshire, UK).

Measurement of O_2 consumption, CO_2 production, and energy expenditure

Metabolic parameters, O_2 consumption (VO_2), CO_2 production (VCO_2), and energy expenditure, of control (*A/A;fTg/0*) and *AgRP*$^{eIF2\alpha A/A}$ mice were analyzed using an indirect calorimetry system. VO_2 and VCO_2 were measured at 10 min intervals for each mouse. Mice were acclimated in the chambers for 72 h prior to data collection. The average values during the light and dark periods were calculated. Data acquisition and instrument control were coordinated by MetaScreen software, and the obtained raw data were processed using ExpeData.

Real-time PCR

RNA was isolated from hypothalami using Trizol reagent (Sigma-Aldrich) or immunoprecipitation with HA antibody, as explained above, and reverse transcribed with MMLV reverse transcriptase (Beams Biotechnology, Gyeonggi-do, Korea). Gene expression was measured by real-time PCR using Evagreen qPCR Mastermix

(TApplied Biological Materials Inc., Richmond, BC, Canada). The primers used were as follows: Agrp sense primer, 5'-CAG GTC TAA GTC TGA ATG GC-3'; Agrp antisense primer, 5'-GGA CTC GTG CAG CCT TAC-3'; Pomc sense primer, 5'-GCT TCA GAC CTC CAT AGA TGT-3'; Pomc antisense primer, 5'-TTG CCA GGA AACACG GG-3'; Aft4 sense primer, 5'-ATG GCC GGC TAT GGA TGA T-3'; Aft4 antisense primer, 5'-CGA AGT CAA ACT CTT TCA GAT CCA TT-3'; Chop sense primer, 5'-CTG CCT TTC ACC TTG GAG AC-3'; Chop antisense primer, 5'-CGT TTC CTG GGG ATG AGA TA-3'; Bip sense primer, 5'-GGT GCA GCA GGA CAT CAA GTT-3'; Bip antisense primer, 5'-CCC ACC TCC AAT ATC AAC TTG A-3'; Xbp1 total sense primer, 5'-AAG AAC ACG CTT GGG AAT GG-3'; Xbp1 total antisense primer, 5'- ACT CCC CTT GGC CTC CAC-3'; Xbp1 splicing sense primer, 5'-GAG TCC GCA GCA GGT G-3'; Xbp1 splicing antisense primer, 5'- GTG TCA GAG TCC ATG GGA-3'; Atf6 sense primer, 5'-TCG GTC AGT GGA CTC TTA TT-3'; Atf6 antisense primer, 5'-CCA GTG ACA GGC TTA TCT TC-3'; LC3β sense primer, 5'-ACA AAG AGT GGA AGA TGT CCG GCT-3'; LC3β antisense primer, 5'-TGC AAG CGC CGT CTG ATT ATC TTG-3'; Atg5 sense primer, 5'-TAG AAT ATA TCA GAC CAC GAC G-3'; Atg5 antisense primer, 5'-CTC CTC TTC TCT CCA TCT TC-3'; Atg7 sense primer, 5'-TCC GTT GAA GTC CTC TGC TT-3'; Atg7 antisense primer, 5'- CCA CTG AAG TTC ACC ATC CT-3'; Cd36 sense primer, 5'-TGC TGG AGC TGT TAT TGG TG-3'; Cd36 antisense primer, 5'-TGG GTT TTG CAC ATC AAA GA -3'; Beclin1 sense primer, 5'-GGC CAA TAA GAT GGG TCT GA-3'; Beclin1 antisense primer, 5'-GCT GCA CAC AGT CCA GAA AA-3'; Cpt1a sense primer, 5'-CTG GCC TAC TCA GAG GAT GGA-3'; Cpt1a antisense primer, 5'-AAA GGT GTC AAA TGG GAA GGA-3'; Ucp2 sense primer, 5'-CTA CAA GAC TGC ACG AGA GG-3'; Ucp2 antisense primer, 5'-AGC TGC TCA GTG ACA AAC AT-3'; Drp1 sense primer,

5’-TCA CCC GGA GAC CTC TCA TT-3’; Drp1 antisense primer, 5’-TGC TTC AAC TCC ATT TTC TTC TCC-3’; Fis1 sense primer, 5’-ACG AAG CTG CAA GGA ATT TTG A-3’; Fis1 antisense primer, 5’-AAC CAG GCA CCA GGC ATA TT-3’; Opa1 sense primer, 5’-TCT GAG GCC CTT CTC TTG TT-3’; Opa1 antisense primer, 5’-TCT GAC TTC CTG TAA TGC T-3’; Mnf1 sense primer, 5’-TTG CCA CAA GCT GTG TTC GG-3’; Mnf1 antisense primer, 5’-TCT AGG GAC CTG AAA GAT GGG C-3’; Mnf2 sense primer, 5’-AGA GGC AGT TTG AGG AGT GC-3’; Mnf2 antisense primer, 5’-ATG ATG AGA CGA ACG GCC TC-3’; Gfap sense primer, 5’-CAG ACT TTC TCC AAC CTC CAG-3’; Gfap antisense primer, 5’-AAT CTG GTG AGC CTG TAT TGG-3’; β-actin antisense primer, 5’-GGG GTG TTG AAG GTC TCA AA-3’; L19 sense primer, 5’-GGT GAC CTG GAT GAG AAG GA-3’; L19 antisense primer, 5’-TTC AGC TTG TGG ATG TGC TC-3’. Real-time PCR was performed using the StepOnePlus^{TM} Real-Time PCR System (Applied Biosystems, Foster City, CA, USA) for ~40 cycles. Relative mRNA expression was normalized with the β-actin or L19 mRNA level and calculated using the $2^{-\Delta\Delta CT}$ method [31].

Statistical analyses

Statistical analyses were performed in GraphPad Prism 5 software (GraphPad Software, San Diego, CA, USA). All data are expressed as the mean ± SEM. The statistical significance between two groups was analyzed by unpaired Student’s t-test. Two-way analysis of variance (ANOVA) analyses followed by Bonferroni post-hoc testing were performed to detect the significance of differences between two genotypes.

Results

Hypothalamic eIF2α phosphorylation is increased during food deprivation.

To interrogate whether eIF2α signaling is involved in the central regulation of energy balance, I first observed the phosphorylated eIF2α in the mice brain. The phosphorylated eIF2α was observed in various brain regions including the hypothalamus, hippocampus and cortex. In the hypothalamus, phosphorylated eIF2α was observed in the arcuate nucleus (ARC), paraventricular nucleus (PVN), dorsomedial hypothalamic nucleus (DMH) and ventromedial hypothalamic nucleus (VMH) (Figure. 1A). In order to verify whether hypothalamic eIF2α phosphorylation responds to energy status, I analyzed change of hypothalamic eIF2α phosphorylation in different feeding conditions. The eIF2α phosphorylation was increased in hypothalamus of fasted mice compared to fed mice (Figure. 1B), indicating that hypothalamic eIF2α phosphorylation is closely related to energy deprivation. Since hypothalamic AgRP neurons play a critical role in energy homeostasis during food deprivation [4, 7], I further ascertained whether eIF2α phosphorylation in the hypothalamic AgRP neurons is changed on the fasting condition. Interestingly, I found that eIF2α phosphorylation in NPY neurons, which also expressed the AgRP, was increased in fasted mice compared to fed mice (Figure 1C, D).

Next, I determined the effect of eIF2α phosphorylation on feeding behavior after fasting. An ip injection of ISRIB, which blocks eIF2α phosphorylation signaling by promoting eIF2B activity, effectively reduced food intake for 1 h and 4 h after overnight fasting compared to vehicle (Figure 1E). Additionally, c-Fos-positive NPY neurons were significantly decreased by ISRIB injection after overnight fasting (Figure 1F, G). In contrary, An icv injection of salubrinal, which prevent dephosphorylation of

phosphorylated eIF2α by inhibition of phosphatase complexs, increased food intake for 1 h and 4 h after injection compared to vehicle (Figure 1H). In addition, salubrinal increased c-Fos-positive NPY neurons at 1 h after injection compared to vehicle (Figure 1I, J). Collectively, these observations demonstrate that hypothalamic eIF2α phosphorylation could play a role in the response to energy deprivation and might be related to fasting-induced activation of hypothalamic AgRP neurons for the regulation of feeding behavior.

eIF2α phosphorylation in hypothalamic AgRP neurons is associated with feeding behavior and neuronal activation after food deprivation

To determine the role of eIF2α phosphorylation in hypothalamic AgRP neurons on food deprivation-induced feeding behavior, I generated the eIF2α phosphorylation deficient mice specifically in the hypothalamic AgRP neurons (*AgRP*$^{eIF2\alpha A/A}$ mice), which was generated by crossing *eIF2α* homozygous mutant (*eIF2α A/A*) mice bearing floxed wild-type eIF2α transgene (fTg) (*A/A;fTg/Tg*) with mice expressing Cre recombinase in the AgRP neurons (Figure 2A). Since Cre recombinase deletes the transgene and coordinates the expression of EGFP in the AgRP neurons, EGFP signals were observed in *AgRP*$^{eIF2\alpha A/A}$ mice, but not in control mice (Figure 2B). Moreover, 96% of AgRP neurons labelled with tdTomato signals expressed the EGFP in the ARC of AgRP$^{eIF2\alpha A/A}$ mice, as shown by immunohistochemistry analyses (Figure 2C, D).

Next, I analyzed the activation of c-Fos, a molecular marker for the neuronal activity, in hypothalamic ARC of *AgRP*$^{eIF2\alpha A/A}$ mice and control mice after overnight fasting. *AgRP*$^{eIF2\alpha A/A}$ mice revealed a decrease in c-Fos activity in the ARC compared to control mice after overnight fasting (Figure 2E, F). Similarly, *AgRP*$^{eIF2\alpha A/A}$ mice showed a

significant decrease in food intake, meal size and meal duration compared to control mice for 12 h after overnight fasting, but did not show any difference in meal number (Figure 2G-J). Furthermore, fasting condition induced a decrease in the number and intensity of AgRP fibers in the PVN of the *AgRP*$^{eIF2\alpha A/A}$ mice compared to control mice (Figure 2K-M), whereas the number and intensity of α-MSH fibers in the PVN were increased in *AgRP*$^{eIF2\alpha A/A}$ mice compared to control mice. (Figure 2N-P). Taken together, these findings suggest that eIF2α phosphorylation in AgRP neurons plays an important role in AgRP neuronal activity and food intake.

AgRP$^{eIF2\alpha A/A}$ mice show enhanced responsiveness to leptin and attenuated ghrelin sensitivity

To further determine whether eIF2α phosphorylation in hypothalamic AgRP neurons is involved in the leptin-induced energy balance, I investigated the responsiveness of *AgRP*$^{eIF2\alpha A/A}$ mice to leptin after overnight fasting. Interestingly, *AgRP*$^{eIF2\alpha A/A}$ mice displayed significantly decreased food intake in response to leptin (1 μg/2 μl) compared to control mice (Figure 3A). Accordingly, this low dose of leptin resulted in a greater decrease of body weight in the *AgRP*$^{eIF2\alpha A/A}$ mice than in control mice (Figure 3B).

Because the phosphorylation of signal transducer and activator of transcription 3 (STAT3) is a molecular indicator to evaluate the activity of leptin signaling pathway, I determined leptin-induced STAT3 phosphorylation (pSTAT3) in the control and *AgRP*$^{eIF2\alpha A/A}$ mice. The leptin-induced level of pSTAT3 was significantly higher in the *AgRP*$^{eIF2\alpha A/A}$ mice than control mice (Figure 3C, D). Furthermore, leptin induced a

greater increase in the number and intensity of α-MSH fibers in the PVN of the *AgRP*$^{eIF2\alpha A/A}$ mice than control mice (Figure 3E-G). To further determine whether eIF2α phosphorylation in AgRP neurons affects sensitivity of ghrelin, I investigated the responsiveness of *AgRP*$^{eIF2\alpha A/A}$ mice to ghrelin. Interestingly, *AgRP*$^{eIF2\alpha A/A}$ mice revealed a significant decrease in food intake for 1 h and 2 h after injection of ghrelin compared to control mice (Figure 3H, I). Collectively, these observations suggest that eIF2α phosphorylation in the hypothalamic AgRP neurons is closely correlated with leptin and ghrelin responsiveness.

AgRP$^{eIF2\alpha A/A}$ mice show reduced food intake and increased energy expenditure

To identify whether eIF2α phosphorylation in the hypothalamic AgRP neurons is important in the control of the whole-body energy balance, the metabolic parameters of both control and *AgRP*$^{eIF2\alpha A/A}$ mice was investigated under the normal diet condition. The *AgRP*$^{eIF2\alpha A/A}$ mice revealed a significant decrease in body weight and food intake compared to control mice (Figure 4A, B). Along with the difference in body weight during normal diet condition, the peripheral metabolic organ, such as the liver and perirenal fat, of the *AgRP*$^{eIF2\alpha A/A}$ mice weighted less than those of the control mice (Figure 4C). The *AgRP*$^{eIF2\alpha A/A}$ mice also showed significant elevations of VO_2, VCO_2, and energy expenditure compared with control mice (Figure 4D-H). Furthermore, the deficiency of eIF2α phosphorylation in AgRP neurons resulted in a decreased number and intensity of AgRP fibers in the PVN compared to control mice (Figure 4I-K), whereas number and intensity of α-MSH fibers in the PVN were greater in *AgRP*$^{eIF2\alpha A/A}$ mice than control mice (Figure 4L-N). These results indicate that deficiency of eIF2α

phosphorylation in AgRP neurons causes reduction of body weight by affecting food intake and energy expenditure during normal diet condition.

Food deprivation-induced UPR signaling in hypothalamic AgRP neurons is attenuated in *AgRP*$^{eIF2\alpha A/A}$ mice.

It has been established that the ER stress-induced UPR signaling in the hypothalamus is associated with diverse metabolic responses, as a key mediator of energy balance [23, 25, 28]. Therefore, I investigated the ER stress-induced the UPR signaling in the hypothalamic AgRP and POMC neurons. I used a Ribo-Tag system of transgenic (*AgRP-Cre;Rpl22*^{HA} and *POMC-Cre;Rpl22*^{HA}) mice that expressed HA-tagged ribosomal protein Rpl22 in AgRP or POMC neurons to identify the gene expression specifically in AgRP or POMC neurons. The IHC analysis identified specific HA signals in the AgRP neurons in the hypothalamus of *AgRP-Cre;Rpl22*^{HA} mice (Figure 5A). Real-time PCR using the Ribo-Tag system further revealed that HA-mediated immunoprecipitation occurred in the cells expressing AgRP or in the cells expressing POMC, but not in those producing GFAP (marker for astrocyte) (Figure 5B, C). The expression of UPR genes was increased in AgRP neurons by fasting (Figure 5D). However, I did not find any difference in UPR genes expression in the POMC neurons between fasted mice and fed mice (Figure 5E). These findings suggest that ER stress-induced UPR signaling was activated in hypothalamic AgRP neurons specifically after overnight fasting.

To investigate whether eIF2α phosphorylation in AgPR neurons affects fasting-induced expression of the UPR genes, I analyzed the mRNA purified with Ribo-Tag

system in AgRP neurons of both *AgRP*$^{eIF2\alpha A/A}$*;Rpl22*^{HA} mice and control mice (*AgRP-Cre;Rpl22*^{HA} mice) after overnight fasting. Interestingly, expression of UPR genes in AgRP neurons was significantly lower in *AgRP*$^{eIF2\alpha A/A}$ mice than control mice after overnight fasting (Figure 5F), suggesting that eIF2α phosphorylation in hypothalamic AgRP neurons is required for normalcy in expression of UPR genes in the AgRP neurons during fasting condition.

It has been well established that induction of autophagy and mitochondrial dynamics in hypothalamic AgRP neurons affects the energy homeostasis through regulation of AgRP neuron activation during food deprivation [12, 13]. Therefore, I measured changes in expression of genes for autophagy and mitochondrial dynamics in AgRP neurons of both control and *AgRP*$^{eIF2\alpha A/A}$ mice after overnight fasting using Ribo-tag system. *AgRP*$^{eIF2\alpha A/A}$ mice showed a significant decrease in expression of autophagy genes (Figure 5G) and mitochondrial genes (Figure 5H) in hypothalamic AgRP neurons after overnight fasting. Agrp expression was also decreased in *AgRP*$^{eIF2\alpha A/A}$ mice compared control mice after overnight fasting (Figure 5I).

Taken together, the current findings suggest that eIF2α phosphorylation in AgRP neurons is a crucial contributor of the fasting-induced UPR signaling in AgRP neurons, which may affect the activation of AgRP neurons through induction of autophagy and mitochondrial dynamics in a low energy condition.

Figures

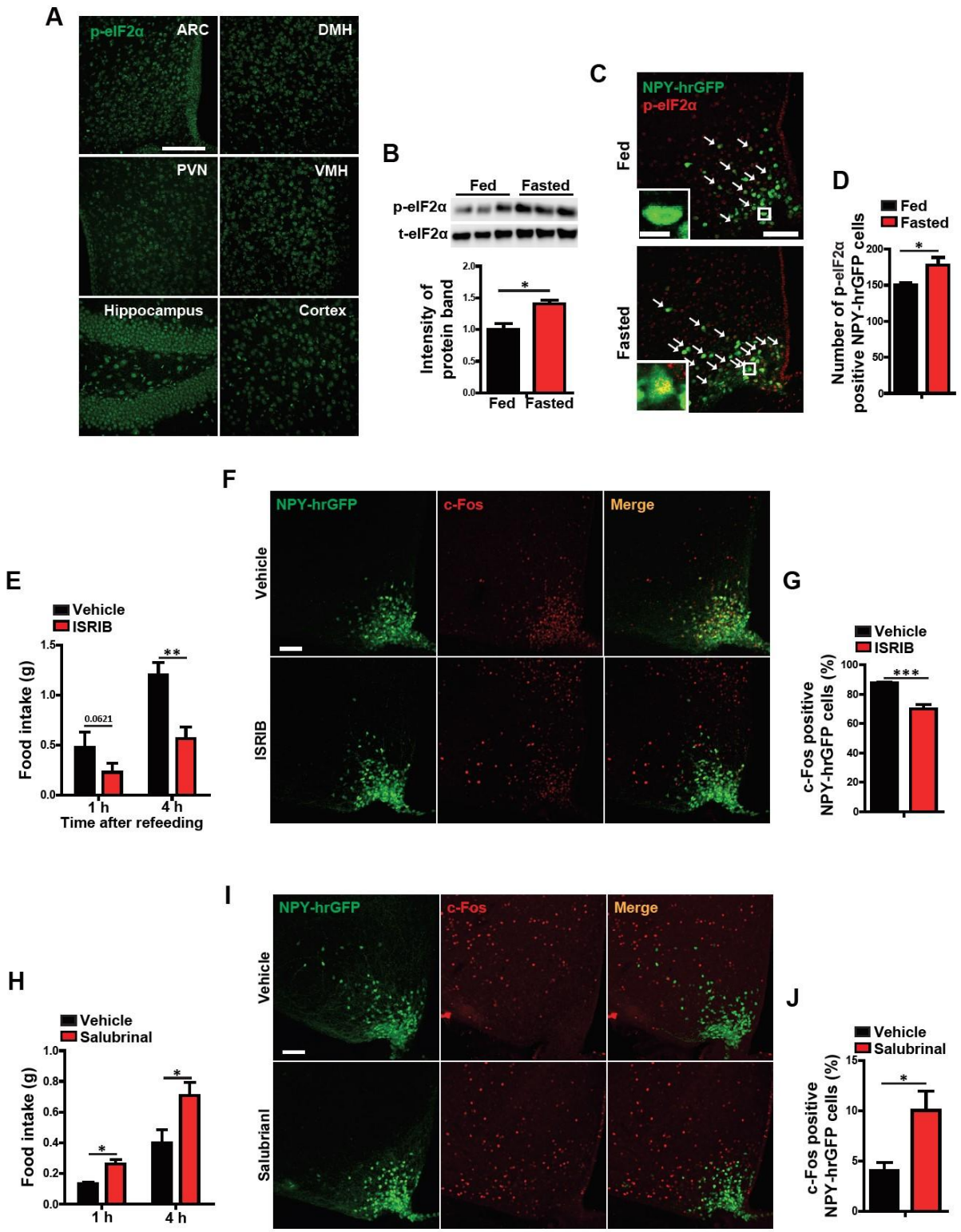
A
p-eIF2α
ARC
DMH
PVN
VMH
Hippocampus
Cortex
B
Fed
Fasted
p-eIF2α
t-eIF2α
Intensity of protein band
Fed
Fasted
C
NPY-hrGFP
p-eIF2α
Fed
Fasted
D
Fed
Fasted
Number of p-eIF2α positive NPY-hrGFP cells
E
Vehicle
ISRIB
Food intake (g)
0.0621
1 h
4 h
Time after refeeding
F
NPY-hrGFP
c-Fos
Merge
Vehicle
ISRIB
G
Vehicle
ISRIB
c-Fos positive NPY-hrGFP cells (%)
H
Vehicle
Salubrinal
Food intake (g)
1 h
4 h
I
NPY-hrGFP
c-Fos
Merge
Vehicle
Salubrianl
J
Vehicle
Salubrinal
c-Fos positive NPY-hrGFP cells (%)

Figure 1. Hypothalamic eIF2α phosphorylation is changed by energy status.

(A) Representative images show the phosphorylated eIF2α in the hypothalamic arcuate nucleus (ARC), dorsomedial hypothalamic nucleus (DMH), ventromedial hypothalamic nucleus (VMH) and paraventricular hypothalamic nucleus (PVN), hippocampus and cortex of mice under normal diet condition. (B) Immunoblot analyses show a marked increase in eIF2α phosphorylation in the hypothalamus of fasted mice compared to fed mice (n=3/group). (C, D) Representative images (C) and calculated graphs (D) show that NPY neurons expressing phosphorylated eIF2α were increased in the ARC by fasting (n=4 sections of 2 mice/group). To confirm effect of eIF2α phosphorylation on food intake and activation of NPY/AgRP neurons, mice were injected with ISRIB that inhibits the effects of eIF2α phosphorylation at 90 min before refeeding after overnight fasting. ISRIB inhibited fasting-induced food intake (E, n=4/group) and c-Fos activation of the NPY neurons (F, G, n=4 sections of 2 mice/group) in the hypothalamic ARC. Salubrinal that prevent dephosphorylation of phosphorylated eIF2α increased food intake (H) and c-Fos activation of the NPY neurons (I, J, n=4 sections of 2 mice/group) in the hypothalamic ARC. Data are presented as mean ± SEM. $^{*}p<0.05$, $^{**}p<0.01$ and $^{***}p<0.001$. Scale bar = 100 μm (20 μm for higher magnification view in insets).

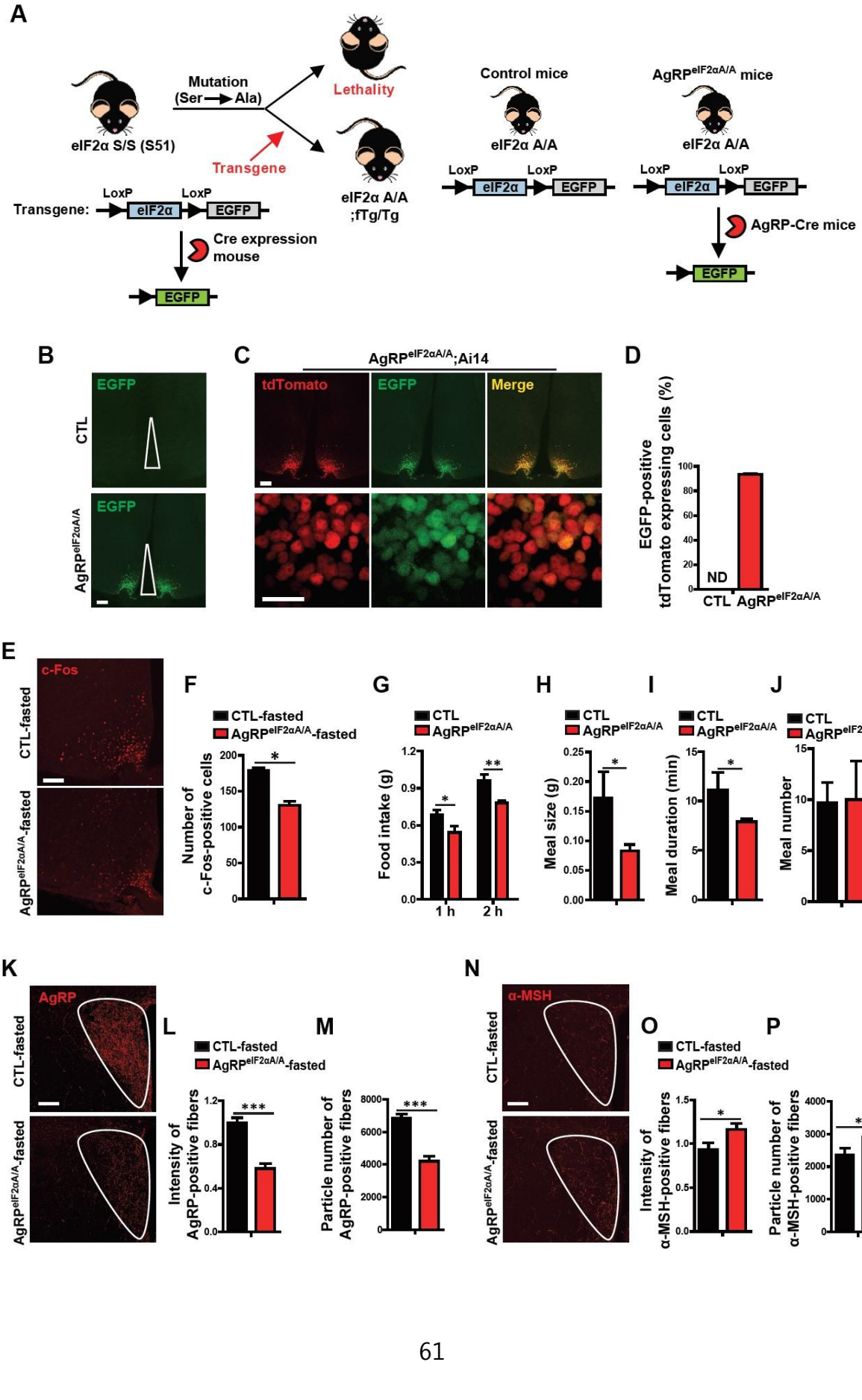
A
eIF2α S/S (S51)
Mutation
(Ser → Ala)
Lethality
Transgene
eIF2α A/A
;fTg/Tg
Transgene:
LoxP
eIF2α
LoxP
EGFP
Cre expression
mouse
Control mice
eIF2α A/A
AgRP^eIF2αA/A mice
eIF2α A/A
AgRP-Cre mice
B
CTL
AgRP^eIF2αA/A
EGFP
C
AgRP^eIF2αA/A;Ai14
tdTomato
EGFP
Merge
D
EGFP-positive
tdTomato expressing cells (%)
ND
CTL
AgRP^eIF2αA/A
E
c-Fos
CTL-fasted
AgRP^eIF2αA/A-fasted
F
CTL-fasted
AgRP^eIF2αA/A-fasted
Number of
c-Fos-positive cells
G
CTL
AgRP^eIF2αA/A
Food intake (g)
1 h
2 h
H
Meal size (g)
I
Meal duration (min)
J
Meal number
K
AgRP
L
Intensity of
AgRP-positive fibers
M
Particle number of
AgRP-positive fibers
N
α-MSH
O
Intensity of
α-MSH-positive fibers
P
Particle number of
α-MSH-positive fibers

Figure 2. Deficiency of eIF2α phosphorylation in AgRP neurons results in attenuation of the neuronal activity and feeding behavior after food deprivation.

(A) Diagram depicts generation of mice with deficiency of eIF2α phosphorylation in AgRP neurons (*AgRP*$^{eIF2\alpha A/A}$ mice). (B) Representative images show expression of enhanced green fluorescence protein (EGFP) in the hypothalamus of *AgRP*$^{eIF2\alpha A/A}$ mice and control (*A/A;fTg/0*) mice. (C, D) Representative images (C) and calculated data (D) showing co-expression of AgRP-specific tdTomato signals and EGFP in the hypothalamic ARC of *AgRP*$^{eIF2\alpha A/A}$*;Ai14* mice (n=8 sections of 4 mice/group). (E, F) Immunohistochemical analyses of neuronal activity in the hypothalamic ARC of control and *AgRP*$^{eIF2\alpha A/A}$ mice using c-Fos antibody. Representative images (E) and calculated data (F) show the fasting-induced c-Fos-positive cells in ARC of *AgRP*$^{eIF2\alpha A/A}$ mice compared with control mice (n=6 sections of 2 mice/group). (G-J) Feeding parameters were measured in *AgRP*$^{eIF2\alpha A/A}$ mice and control mice after overnight fasting. (G) Food intake was measured for 1 h and 2 h after fasting (n=8-11/group). Average meal size (H), average meal duration (I) and meal number (J) were measured for 12 h after overnight fasting (n=3/group). (K-P) Change in AgRP and α-MSH innervation was determined in the PVN of *AgRP*$^{eIF2\alpha A/A}$ mice and control mice after overnight fasting. Representative images show AgRP immuno-positive signals (K) and α-MSH immuno-positive signals (N) in the PVN after overnight fasting. Fasting-induced intensity (L) and particle number (M) of AgRP fiber signals were significantly decreased in *AgRP*$^{eIF2\alpha A/A}$ mice compared to control mice, whereas intensity (O) and particle number (P) of α-MSH fiber signals were greater in *AgRP*$^{eIF2\alpha A/A}$ mice than in control mice (n=4 sections of 2 mice/group). Data are presented as mean ± SEM. $^{*}p<0.05$, $^{**}p<0.01$ and $^{***}p<0.001$. Scale bar = 100 μm.

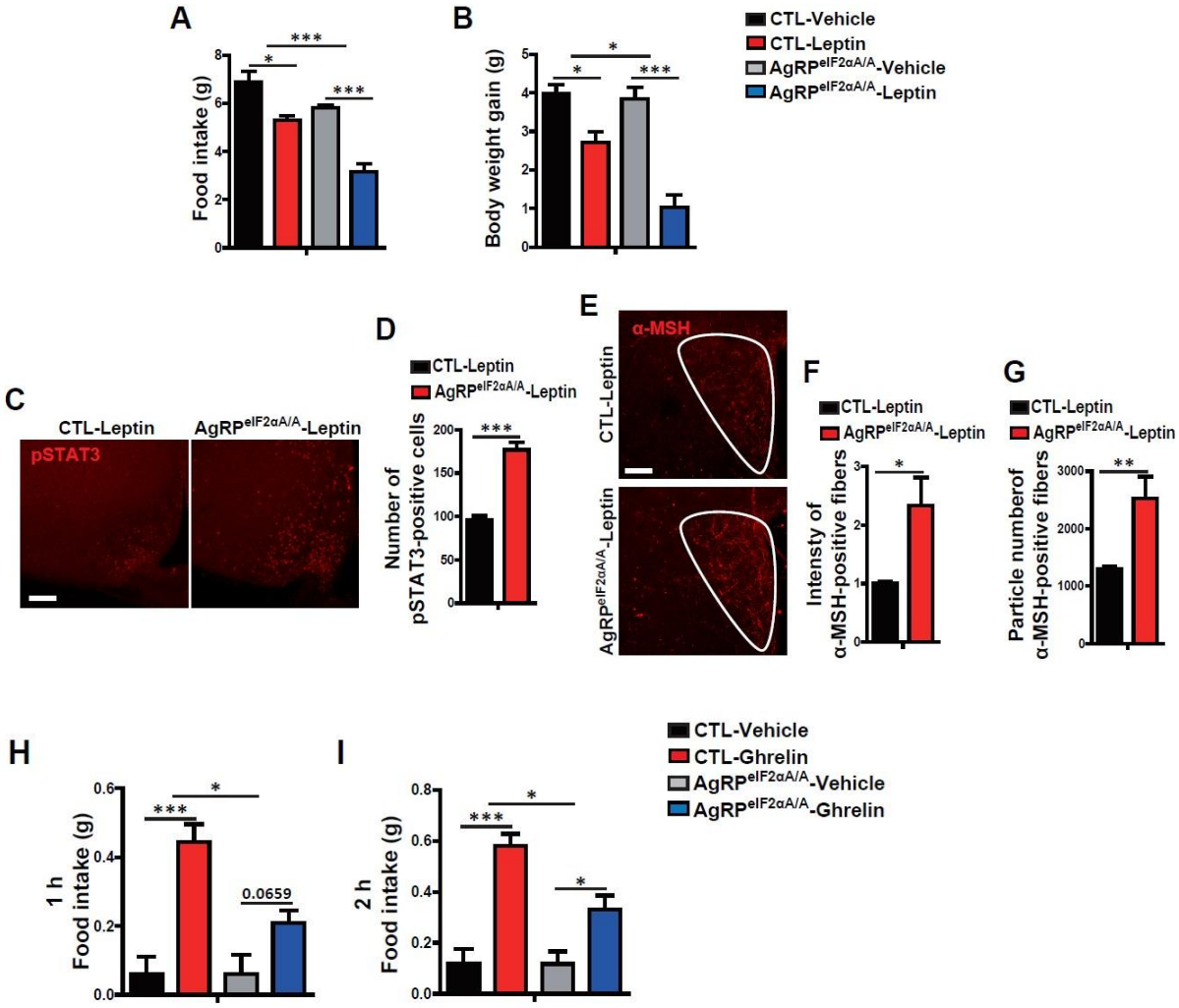

Figure 3. *AgRP*$^{eIF2αA/A}$ mice show an enhanced sensitivity to leptin and an attenuated sensitivity to ghrelin

(A, B) To identify the effects of eIF2α phosphorylation deficiency in AgRP neurons (*AgRP*$^{eIF2αA/A}$) on leptin sensitivity, food intake (A) and body weight (B) were measured for 24 h after an intracerebroventricular (icv) injection of leptin (1 μg/2 μl) or vehicle

(n=4-7/group). (C, D) Representative images (C) and calculated data (D) show a greater leptin-induced increase in pSTAT3 level in the *AgRP*$^{eIF2\alpha A/A}$ mice than control mice (n=6 sections of 3 mice/group). (E-G) Representative images (E) and calculated data (F, G) reveal that leptin induced a greater increase in α-MSH immuno-positive signals in the PVN of *AgRP*$^{eIF2\alpha A/A}$ mice than in control mice (n=6 sections of 3 mice/group). To determine the sensitivity of ghrelin in *AgRP*$^{eIF2\alpha A/A}$ mice, food intake was measured for 1 h and 2 h after injection of ghrelin (1 μg/2 μl, H, I, n=4/group). Data are presented as mean ± SEM. $^{*}p<0.05$, $^{**}p<0.01$ and $^{***}p<0.001$. Scale bar = 100 μm.

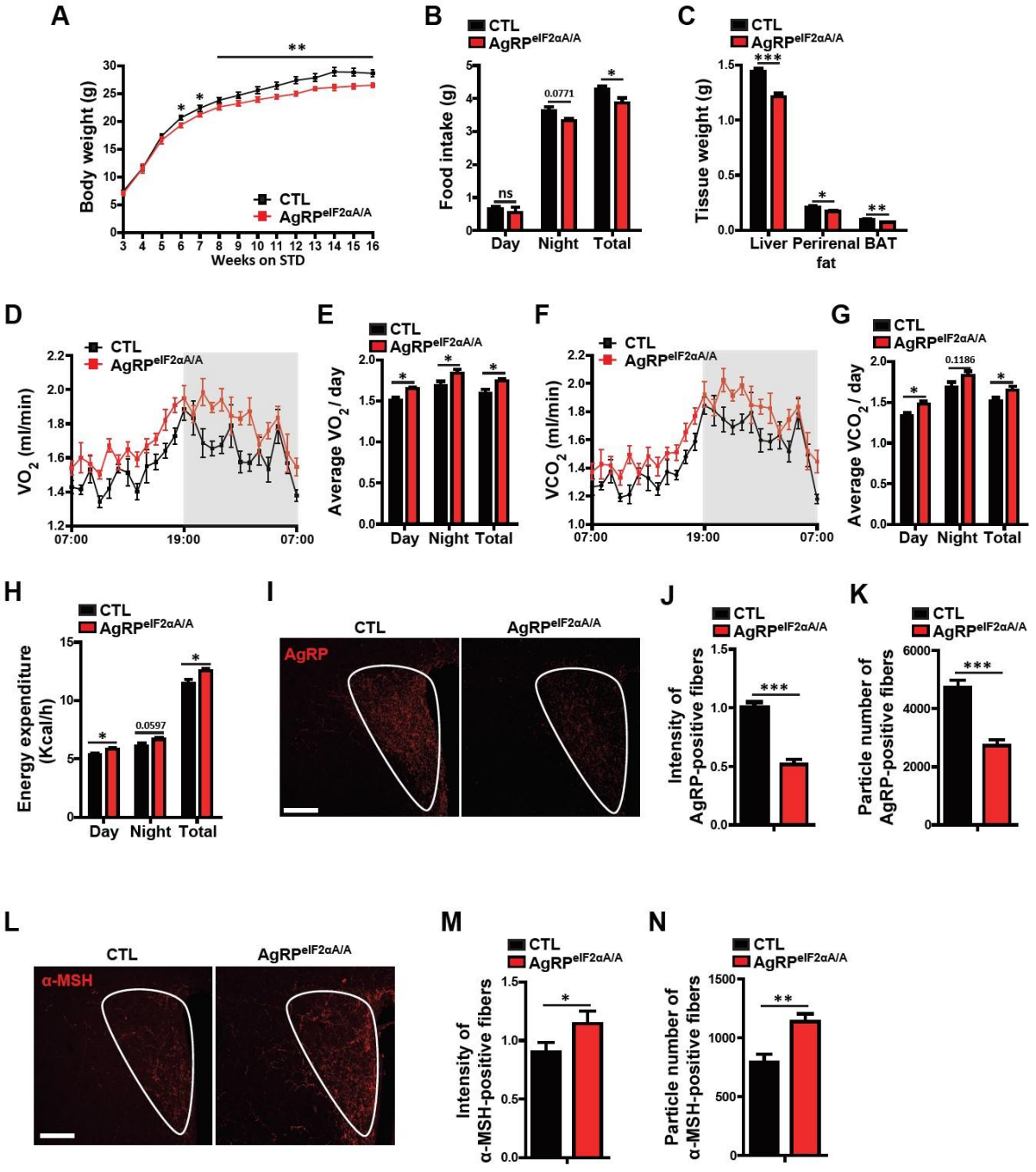
A
Body weight (g)
Weeks on STD
CTL
AgRP^eIF2αA/A
B
Food intake (g)
Day
Night
Total
ns
0.0771
C
Tissue weight (g)
Liver
Perirenal fat
BAT
D
VO2 (ml/min)
07:00
19:00
07:00
E
Average VO2/ day
F
VCO2 (ml/min)
G
Average VCO2/ day
0.1186
H
Energy expenditure (Kcal/h)
0.0597
I
AgRP
J
Intensity of AgRP-positive fibers
K
Particle number of AgRP-positive fibers
L
α-MSH
M
Intensity of α-MSH-positive fibers
N
Particle number of α-MSH-positive fibers

Figure 4. AgPR neuron-specific deficiency of eIF2α phosphorylation reduces the food intake and increases the energy expenditure.

To identify whether eIF2α phosphorylation in the hypothalamic AgRP neurons is important in the control of energy balance, mice were fed a normal diet and were subjected to measurement of metabolic phenotypes. (A) Body weight was significantly lower in *AgRP*$^{eIF2\alpha A/A}$ mice than in control mice (n=8/group). (B) Average daily food intake was measured for a week at 16-17 weeks of age (n=8/group). (C) Fat mass was measured at 16 weeks of age (n=8/group). BAT=brown adipose tissue. (D-H) Indirect calorimetry measurements were performed in metabolic cages to determine changes in the oxygen consumption (VO2) (D, E), carbon dioxide generation (VCO2) (F, G) and energy expenditure (H, n=6/group). (I-N) Change in AgRP and α-MSH innervation was determined in the PVN of *AgRP*$^{eIF2\alpha A/A}$ mice and control mice. Representative images show AgRP immuno-positive signals (I) and α-MSH immuno-positive signals (L) in the PVN. Intensity (J) and particle number (K) of AgRP fiber signals were significantly lower in *AgRP*$^{eIF2\alpha A/A}$ mice than in control mice, whereas intensity (M) and particle number (N) of α-MSH fiber signals were greater in *AgRP*$^{eIF2\alpha A/A}$ mice than in control mice (n=6 sections of 2 mice/group). Data are presented as mean ± SEM. $^{*}p<0.05$, $^{**}p<0.01$ and $^{***}p<0.001$. ns=not significant. Scale bar = 100 μm.

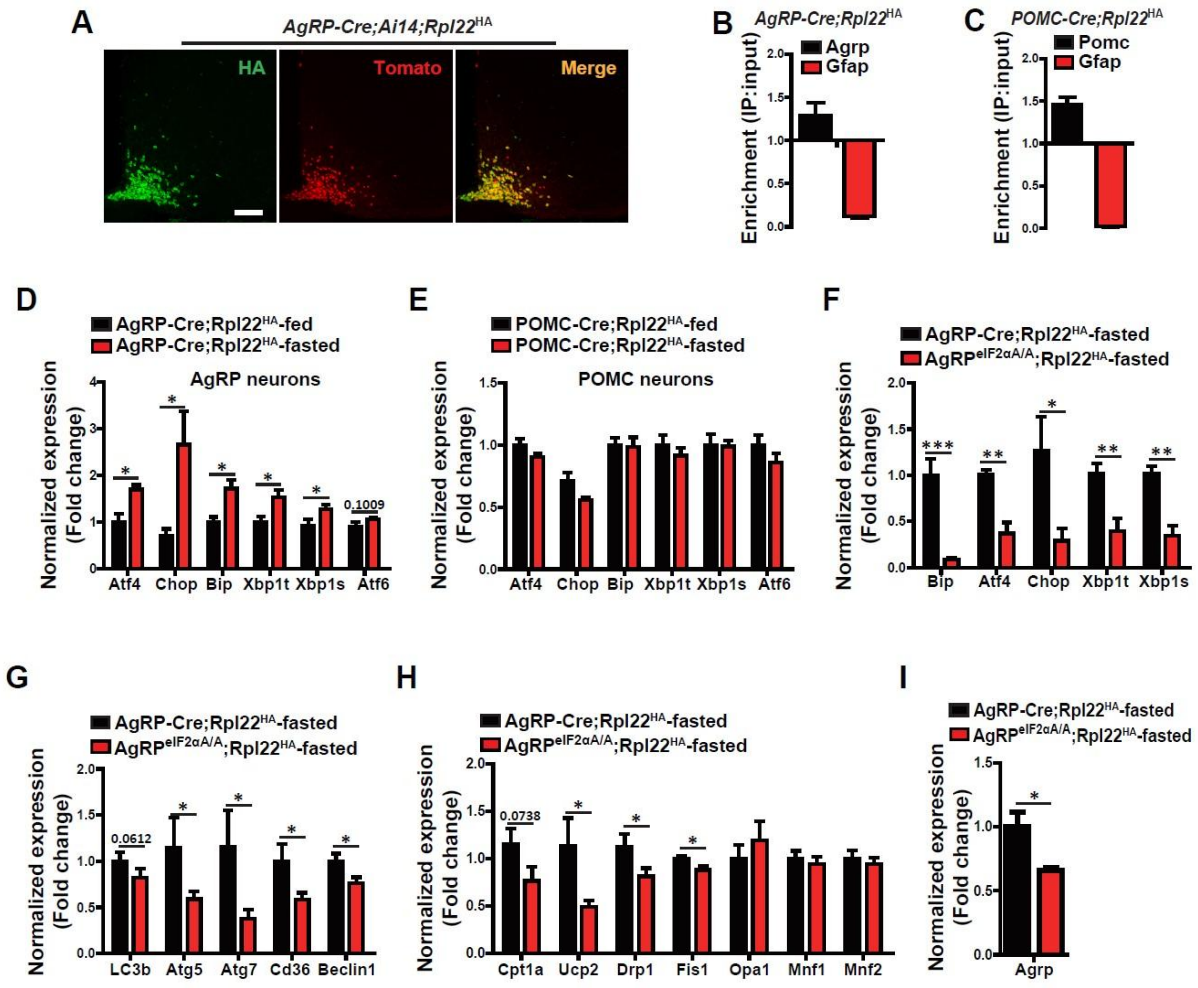

Figure 5. Deficiency of eIF2α phosphorylation in AgRP neurons decreases the fasting-induced UPR signaling and cellular responses in hypothalamic AgRP neurons.

To investigate the expression of genes in AgRP neurons specifically using Ribo-Tag system, transgenic mice (*Rpl22*^{HA}) expressing HA-tagged Rpl22 were crossed with *AgRP*$^{eIF2αA/A}$ mice, which resulted in generation of *AgRP*$^{eIF2αA/A}$;*Rpl22*^{HA} mice. *AgRP-Cre;Rpl22*^{HA} mice were used as the control. To analyze the mRNA specifically

translating in POMC neurons, *POMC-Cre* mice were crossed with *Rpl22*^{HA} mice, resulting in *POMC-Cre;Rpl22*^{HA} mice. (A-C) Ai14 reporter mice were bred with A*gRP-Cre;Rpl22*^{HA} mice for detection of AgPR neurons. (A) Representative images showing co-expression of AgRP-specific tdTomato signals and HA signals in the hypothalamic ARC of *AgRP-Cre;Rpl22*^{HA}*;Ai14* mice (A). (B, C) To assess the cell type specificity of the obtained RNA samples, I analyzed enrichment of Agrp (marker for AgRP purification) and Pomc (marker for AgRP purification) and Gfap (marker for astrocyte contamination) compared to that of input samples (n=3/group). (D, E) Real-time PCR analyses of RNA samples (immunoprecipitated with HA antibody) show the expression of UPR genes (Atf4, Chop, Bip, Xbp1t, Xbp1s and Atf6) from hypothalamic extracts of *AgRP-Cre;Rpl22*^{HA} mice (D) or *POMC-Cre;Rpl22*^{HA} mice (E) after feeding or fasting (n=3/group). (F-J) Since UPR signaling and intracellular responses, such as autophagy and mitochondrial dynamics, in the hypothalamic AgRP neurons were induced by food deprivation, real-time PCR analyses were performed using RNA samples immunoprecipitated with HA antibody to determine the expression UPR genes (F), autophagy genes (LC3b, Atg5, Atg7, Cd36 and Beclin1) (G), genes for mitochondrial dynamics (Ctp1a, Ucp2, Drp1, Fis1, Opa1, Mnf1 and Mnf2) (H) and Agrp (I) in the hypothalamic AgRP neurons of *AgRP*$^{eIF2\alpha A/A}$;*Rpl22*^{HA} mice and control mice (*AgRP-Cre;Rpl22*^{HA} mice) after overnight fasting (n=3/group). Data are presented as mean ± SEM. $^{*}p<0.05$, $^{**}p<0.01$ and $^{***}p<0.001$. Scale bar = 100 μm.

Discussion

In the present study, I found that hypothalamic eIF2α phosphorylation was increased during food deprivation and that eIF2α phosphorylation influenced the activation of AgRP neurons and the feeding behavior. The current observations demonstrate that eIF2α phosphorylation in hypothalamic AgRP neurons is a critical contributor to the activation of AgRP neurons and feeding behavior through the modulation of ER stress-induced UPR signaling and metabolic-relative cellular responses, such as autophagy and mitochondrial dynamics, in the AgRP neurons during food deprivation.

Whole-body energy balance is linked to the communication between the central compartments and the peripheral organs [1, 2]. Moreover, it has been recognized that the circuit of hypothalamic AgRP and POMC neurons is the master unit to mediate the effect of metabolism-related messengers such as adiposity signals and gut-derived hormones [5, 7]. Thus, the ability to sense the energy status of hypothalamic AgRP and POMC neurons is important for whole-body energy metabolism. In particular, several reports have highlighted function of eIF2α signaling in the various cell types, such as pancreatic beta cells and hepatocytes which was shown to be essential for the maintenance of cellular homeostasis in target cells [22, 23]. Recently, it was reported that the eIF2α signaling in the brain is associated with neuronal degeneration as well as control of feeding [24]. Furthermore, ER stress-induced eIF2α phosphorylation during over-nutrition caused attenuation of the hypothalamic POMC processing for α-MSH production, which resulted in the diet-induced obesity [28].

However, the effect of eIF2α signaling in AgRP neurons on energy status has received less attention than in POMC neurons. In this study, I focused on the function of eIF2α phosphorylation in the hypothalamic AgRP neurons as a mediator of whole-

body energy metabolism during food deprivation. Interestingly, I found that hypothalamic eIF2α phosphorylation was increased during fasting and that inhibition of eIF2α phosphorylation reduced the food intake after overnight fasting, suggesting that eIF2α phosphorylation in the hypothalamus is associated with the change of energy status and affects the feeding behavior. During food deprivation, enhanced AgRP neuron activity in the hypothalamus compensates the energy homeostasis through promoting the feeding behavior and inhibiting energy expenditure [7, 8]. In the current study, I observed that food intake was significantly decreased in *AgRP*$^{eIF2\alpha A/A}$ mice compared to control mice after overnight fasting and that deficiency of eIF2α phosphorylation in AgRP neurons decreased the fasting-induced neuronal activity in the hypothalamic ARC. These changes might be due to a decrease in fasting-induced activation of AgRP neurons caused by AgRP neuron-specific deficiency of eIF2α phosphorylation, which results in the decreased food intake after overnight fasting. In this study, I focused on the role of eIF2α phosphorylation in the hypothalamic AgRP neurons during food deprivation. However, I could not exclude a possible change of eIF2α phosphorylation in other regions of the hypothalamus such as PVN and VMH during food deprivation. Therefore, further studies are required to identify the role of region-specific eIF2α phosphorylation in the hypothalamus during energy deprivation.

The leptin released from adipose tissues is an important anorexigenic hormone in the control of energy balance. Leptin signaling activates the POMC neurons and inhibits the AgRP neurons by stimulating STAT3 phosphorylation (pSTAT3) [32, 33]. In our study, *AgRP*$^{eIF2\alpha A/A}$ mice showed metabolic phenotypes indicating increased responsiveness to leptin, and they revealed the induction of molecular indicators that demonstrate leptin responsiveness, such as leptin-induced pSTAT3 in the ARC and α-

MSH innervation to the PVN. It is wll-known that the POMC neurons receive inhibitory projections from activated AgRP neurons during energy deprivation, which promote the feeding behavior [5, 8]. Interestingly, deficiency of eIF2α phosphorylation in AgRP neurons resulted in a decrease in the AgRP neuropeptide in the AgRP nerve terminal at PVN after overnight fasting, thereby enhancing the effect of POMC neurons during food deprivation. Therefore, these changes might affect the increased leptin sensitivity in *AgRP*$^{eIF2\alpha A/A}$ mice, which resulted in a decreased food intake. Given the importance of leptin sensitivity in energy control, the increased leptin sensitivity might contribute to decreased food intake and enhanced energy expenditure in the *AgRP*$^{eIF2\alpha A/A}$ mice under normal diet. This possibility, however, must be studied in detail in future.

Although studies to understand the functional mechanisms of AgRP neurons during food deprivation have focused on the physiological change of AgRP neurons, the food deprivation-induced intracellular responses in AgRP neurons remain largely unexplored. Several reports have revealed that various cellular stress-induced ER stress in the hypothalamic neurons caused the dysfunction of hypothalamic neurons, which induced metabolic diseases such as obesity and diabetes [25, 27, 28]. Interestingly, recent reports show that hypothalamic AgRP neurons are typically activated by food deprivation, which is associated with ER stress-induced UPR activation in AgRP neurons, but not in POMC neurons [34, 35]. Furthermore, ER stress-induced UPR signaling is associated with cellular responses such as autophagy and mitochondria metabolism [36-38]. These responses in AgRP neurons may play a critical role in energy homeostasis through the regulation of AgRP neuron activity under energy deprivation. In our study, eIF2α phosphorylation deficiency in AgRP neurons decreased fasting-induced UPR signaling in the hypothalamic AgRP neurons.

Furthermore, the expression of autophagy genes and genes for mitochondrial dynamics was significantly decreased in *AgRP*$^{eIF2\alpha A/A}$ mice after overnight fasting. In line with previous reports, these results indicate that eIF2α phosphorylation signaling in hypothalamic AgRP neurons affected the fasting-induced activation of AgRP neurons through regulation of UPR signaling that affects the autophagy and mitochondrial dynamics during fasting condition.

In summary, this study newly identified eIF2α phosphorylation in hypothalamic AgRP neurons as a key mediator in the control of energy balance through regulation of the UPR signaling and cellular responses, which highlights contribution of eIF2α phosphorylation to food deprivation-induced activation of AgRP neurons in the hypothalamus. These observations suggest that eIF2α signaling in AgRP neurons could be an important novel energy sensor.

References

1. Williams KW, Elmquist JK: From neuroanatomy to behavior: central integration of peripheral signals regulating feeding behavior. *Nat Neurosci* 2012, 15:1350-1355.
2. Balthasar N, Dalgaard LT, Lee CE, Yu J, Funahashi H, Williams T, Ferreira M, Tang V, McGovern RA, Kenny CD, et al: Divergence of melanocortin pathways in the control of food intake and energy expenditure. *Cell* 2005, 123:493-505.
3. Roh E, Song DK, Kim MS: Emerging role of the brain in the homeostatic regulation of energy and glucose metabolism. *Exp Mol Med* 2016, 48:e216.
4. Wu Q, Boyle MP, Palmiter RD: Loss of GABAergic signaling by AgRP neurons to the parabrachial nucleus leads to starvation. *Cell* 2009, 137:1225-1234.
5. Dietrich MO, Horvath TL: Hypothalamic control of energy balance: insights into the role of synaptic plasticity. *Trends Neurosci* 2013, 36:65-73.
6. Shutter JR, Graham M, Kinsey AC, Scully S, Luthy R, Stark KL: Hypothalamic expression of ART, a novel gene related to agouti, is up-regulated in obese and diabetic mutant mice. *Genes Dev* 1997, 11:593-602.
7. Thomas MA, Xue B: Mechanisms for AgRP neuron-mediated regulation of appetitive behaviors in rodents. *Physiol Behav* 2018, 190:34-42.
8. Cansell C, Denis RG, Joly-Amado A, Castel J, Luquet S: Arcuate AgRP neurons and the regulation of energy balance. *Front Endocrinol (Lausanne)* 2012, 3:169.
9. Briggs DI, Enriori PJ, Lemus MB, Cowley MA, Andrews ZB: Diet-induced obesity causes ghrelin resistance in arcuate NPY/AgRP neurons. *Endocrinology* 2010, 151:4745-475

10. Goncalves GH, Li W, Garcia AV, Figueiredo MS, Bjorbaek C: Hypothalamic agouti-related peptide neurons and the central melanocortin system are crucial mediators of leptin's antidiabetic actions. *Cell Rep* 2014, 7:1093-1103.
11. Kim MS, Quan W, Lee MS: Role of hypothalamic autophagy in the control of whole body energy balance. *Rev Endocr Metab Disord* 2013, 14:377-386.
12. Kaushik S, Rodriguez-Navarro JA, Arias E, Kiffin R, Sahu S, Schwartz GJ, Cuervo AM, Singh R: Autophagy in hypothalamic AgRP neurons regulates food intake and energy balance. *Cell Metab* 2011, 14:173-183.
13. Dietrich MO, Liu ZW, Horvath TL: Mitochondrial dynamics controlled by mitofusins regulate Agrp neuronal activity and diet-induced obesity. *Cell* 2013, 155:188-199.
14. Wai T, Langer T: Mitochondrial Dynamics and Metabolic Regulation. *Trends Endocrinol Metab* 2016, 27:105-117.
15. Moon SL, Sonenberg N, Parker R: Neuronal Regulation of eIF2alpha Function in Health and Neurological Disorders. *Trends Mol Med* 2018, 24:575-589.
16. Baird TD, Ik RC: Eukaryotic initiation factor 2 phosphorylation and translational control in metabolism. *Adv Nutr* 2012, 3:307-321.
17. Ik RC, Cavener DR: Translational control and the unfolded protein response. *Antioxid Redox Signal* 2007, 9:2357-2371.
18. Ron D, Walter P: Signal integration in the endoplasmic reticulum unfolded protein response. *Nat Rev Mol Cell Biol* 2007, 8:519-529.
19. Teske BF, Ik SA, Bunpo P, Cundiff JK, McClintick JN, Anthony TG, Ik RC: The eIF2 kinase PERK and the integrated stress response facilitate activation of ATF6 during endoplasmic reticulum stress. *Mol Biol Cell* 2011, 22:4390-4405.

20. Adachi Y, Yamamoto K, Okada T, Yoshida H, Harada A, Mori K: ATF6 is a transcription factor specializing in the regulation of quality control proteins in the endoplasmic reticulum. *Cell Struct Funct* 2008, 33:75-89.
21. Majumder M, Huang C, Snider MD, Komar AA, Tanaka J, Kaufman RJ, Krokowski D, Hatzoglou M: A novel feedback loop regulates the response to endoplasmic reticulum stress via the cooperation of cytoplasmic splicing and mRNA translation. *Mol Cell Biol* 2012, 32:992-1003.
22. Choi WG, Han J, Kim JH, Kim MJ, Park JW, Song B, Cha HJ, Choi HS, Chung HT, Lee IK, et al: eIF2alpha phosphorylation is required to prevent hepatocyte death and liver fibrosis in mice challenged with a high fructose diet. *Nutr Metab (Lond)* 2017, 14:48.
23. Back SH, Scheuner D, Han J, Song B, Ribick M, Wang J, Gildersleeve RD, Pennathur S, Kaufman RJ: Translation attenuation through eIF2alpha phosphorylation prevents oxidative stress and maintains the differentiated state in beta cells. *Cell Metab* 2009, 10:13-26.
24. Maurin AC, Benani A, Lorsignol A, Brenachot X, Parry L, Carraro V, Guissard C, Averous J, Jousse C, Bruhat A, et al: Hypothalamic eIF2alpha signaling regulates food intake. *Cell Rep* 2014, 6:438-444.
25. Williams KW, Liu T, Kong X, Fukuda M, Deng Y, Berglund ED, Deng Z, Gao Y, Liu T, Sohn JW, et al: Xbp1s in Pomc neurons connects ER stress with energy balance and glucose homeostasis. *Cell Metab* 2014, 20:471-482.
26. Kim KH, Jeong YT, Oh H, Kim SH, Cho JM, Kim YN, Kim SS, Kim DH, Hur KY, Kim HK, et al: Autophagy deficiency leads to protection from obesity and insulin resistance by inducing Fgf21 as a mitokine. *Nat Med* 2013, 19:83-92.

27. Back SH, Kang SW, Han J, Chung HT: Endoplasmic reticulum stress in the beta-cell pathogenesis of type 2 diabetes. *Exp Diabetes Res* 2012, 2012:618396.
28. Cakir I, Cyr NE, Perello M, Litvinov BP, Romero A, Stuart RC, Nillni EA: Obesity induces hypothalamic endoplasmic reticulum stress and impairs proopiomelanocortin (POMC) post-translational processing. *J Biol Chem* 2013, 288:17675-17688.
29. Sanz E, Yang L, Su T, Morris DR, McKnight GS, Amieux PS: Cell-type-specific isolation of ribosome-associated mRNA from complex tissues. *Proc Natl Acad Sci U S A* 2009, 106:13939-13944.
30. Kang SS, Ebbert MTW, Baker KE, Cook C, Wang X, Sens JP, Kocher JP, Petrucelli L, Fryer JD: Microglial translational profiling reveals a convergent APOE pathway from aging, amyloid, and tau. *J Exp Med* 2018, 215:2235-2245.
31. Livak KJ, Schmittgen TD: Analysis of relative gene expression data using real-time quantitative PCR and the 2(-Delta Delta C(T)) Method. *Methods* 2001, 25:402-408.
32. de Git KC, Adan RA: Leptin resistance in diet-induced obesity: the role of hypothalamic inflammation. *Obes Rev* 2015, 16:207-224.
33. Morris DL, Rui L: Recent advances in understanding leptin signaling and leptin resistance. *Am J Physiol Endocrinol Metab* 2009, 297:E1247-1259.
34. Henry FE, Sugino K, Tozer A, Branco T, Sternson SM: Cell type-specific transcriptomics of hypothalamic energy-sensing neuron responses to weight-loss. *Elife* 2015, 4.
35. Cakir I, Nillni EA: Endoplasmic Reticulum Stress, the Hypothalamus, and Energy Balance. *Trends Endocrinol Metab* 2019, 30:163-176.

36. Senft D, Ronai ZA: UPR, autophagy, and mitochondria crosstalk underlies the ER stress response. *Trends Biochem Sci* 2015, 40:141-148.

37. Nakka VP, Prakash-Babu P, Vemuganti R: Crosstalk Between Endoplasmic Reticulum Stress, Oxidative Stress, and Autophagy: Potential Therapeutic Targets for Acute CNS Injuries. *Mol Neurobiol* 2016, 53:532-544.

38. Bravo R, Gutierrez T, Paredes F, Gatica D, Rodriguez AE, Pedrozo Z, Chiong M, Parra V, Quest AF, Rothermel BA, Lavandero S: Endoplasmic reticulum: ER stress regulates mitochondrial bioenergetics. *Int J Biochem Cell Biol* 2012, 44:16-20.

CHAPTER 3

Guanabenz stimulates appetite and energy expenditure through hypothalamic dopaminergic neurons

Abstract

The hypothalamus integrates various neuronal circuits to regulate feeding and whole-body energy metabolism. The small molecule guanabenz reduces the central sympathetic outflow through stimulation of central α_{2A}-adrenergic receptor and is used as an antihypertensive drug. However, the function of guanabenz in feeding and energy balance is largely unknown. In this study, I evaluated whether the central administration of guanabenz is involved in feeding behavior and energy expenditure. The metabolic parameters, including food intake, body weight and energy expenditure, were acutely increased by administration of guanabenz. Intriguingly, I further identified that hypothalamic dopaminergic neurons were significantly activated by guanabenz. Collectively, the current study suggested that the central administration of guanabenz affects the hypothalamic dopaminergic neuronal activity and regulates feeding and whole-body energy balance.

Introduction

Research over the past decades revealed the importance of the hypothalamus in the control of energy homeostasis and whole-body energy metabolism. In particular, hypothalamic arcuate nucleus (ARC) contains two main neuronal populations: orexigenic neuropeptide Y (NPY)/agouti-related peptide (AgRP) neurons and anorexigenic pro-opiomelanocortin (POMC) neurons. Thus, these neurons in hypothalamic ARC orchestrates feeding behavior and energy expenditure, as well as peripheral glucose metabolism [1-3].

According to recent literature, noradrenaline directly modulates the hypothalamic AgRP and POMC neuronal activity through adrenergic receptors [4]. The α_2-adrenergic receptors constitute a family of G-protein-coupled receptors with three pharmacological subtypes, α_{2A}, α_{2B} and α_{2C}-adrenergic receptors. The α_{2A} and α_{2C} receptors are found mainly in the central nervous system, but α_{2B} receptors are found more frequently on vascular smooth muscle [5, 6]. In addition, α_2-adrenergic receptor signaling is involved in various physiological processes, including regulation of blood pressure, nociception and locomotion [7-9]. Guanabenz, a small molecule that has been shown to act an α_{2A}-adrenergic receptor agonist, was developed as an antihypertensive drug. An antihypertensive effect of guanabenz results from a reduction of central sympathetic outflow through stimulation of central α_{2A}-adrenergic receptor [10, 11]. Central sympathetic nervous system is closely related to food intake and energy expenditure. The activation of sympathetic outflow enhances energy expenditure and reduces food intake [12, 13]. Therefore, at the beginning of this study I tried to identify effect of guanabenz on energy homeostasis in the hypothalamic neurons and found its possible appetite control action through dopaminergic neurons

in ARC.

The dopaminergic neurons are located in several regions of brain, including substantia nigra pars compacta (SNc), ventral tegmental area (VTA) and hypothalamus. These neurons are emerging as a major subset of neurons involved in the integration of neuronal signals to regulate food intake and energy balance [14, 15]. Thus, a growing body of evidence has emerged the physiological change of dopaminergic neurons with the control of food intake [16, 17]. According to the recent literature, neurons expressing tyrosine hydroxylase (TH), an essential enzyme in the pathway for the synthesis of dopamine, in hypothalamic arcuate nucleus (ARC) are associated with the activation of hypothalamic AgRP and POMC neurons involved in energy balance by release of dopamine and GABA in the hypothalamic ARC and paraventricular nucleus (PVN) [18]. However, it is unclear whether adrenergic receptor signaling in hypothalamic dopaminergic neurons affects the energy homeostasis through regulation of dopaminergic neuronal activity.

In this study, I investigated whether central administration of guanabenz affects the feeding behavior and energy expenditure through activation of hypothalamic dopaminergic neurons.

Materials and Methods

Animals

Animals were fed a standard diet (STD, Feedlab, Gyeonggi-Do, Korea) *ad libitum* and given free access to tap water. All animals were maintained in temperature- and humidity-controlled rooms with a 12 h/12 h light-dark cycle, with the lights on from 7:00 a.m. to 7:00 p.m.

Dopamine transporter (DAT)-Cre mice (Stock No.020080) were crossbred with *Rosa26-lox-stop-lox-tdTomato* mice (Ai14 reporter mice, Stock No. 007914) to label DAT-positive cells with tdTomato signals. Indeed, *AgRP-Cre* mice were crossbred with Ai14 reporter mice to detect the AgRP-expressing cells with tdTomato signals. The transgenic mice expressing enhanced green fluorescent protein (EGFP) in POMC neurons (Stock No.009593) were used for immunohistochemical analysis. All animals and procedures used were in accordance with the guidelines and approval of the Institutional Animal Care and Use Committee at the University of Ulsan.

Ribo-Tag system

To analyze mRNA species that are specifically translated in hypothalamic astrocytes, i used the Ribo-Tag translational profiling system [19, 20]. In this study, I used *Rpl22*^{HA} mice (Stock No. 011029, Jackson Laboratory), which have a *loxP*-flanked wild-type exon 4 followed by an identical exon 4 tagged with hemagglutinin (HA), as the Ribo-Tag animal. Crossbreeding Ribo-Tag mice with mice expressing Cre recombinase resulted in the deletion and replacement of the floxed wild-type exon 4 with the HA-tagged exon 4 in cells expressing Cre. The *DAT-Cre* mice were crossbred with *Rpl22*^{HA}

mice to generate *DAT-Cre;Rpl22*^{HA} mice that had both the HA-tagged ribosomal protein Rpl22 and the dopamine transporter-expressing cells.

RNA isolation with the Ribo-Tag system was conducted as previously described [19, 20]. Briefly, dissected hypothalamus samples were collected from animals and homogenized. RNA was extracted from 10% of the cleared lysate and used as input. The remaining lysate was incubated with mouse anti-HA antibody for 4 h at 4°C followed by the addition of protein G agarose beads (LGP-1018B, Lugen, Gyeonggi-Do, Korea) and overnight incubation at 4°C. The beads were washed three times in high salt solution. The bound ribosomes and RNA were separated from the beads with 30 sec of vortexing, and RNA was further purified using a QIAGEN RNeasy Micro Kit (74034, Qiagen, Hilden, Germany). After RNA isolation, I obtained 10–20 ng of RNA sample/hypothalamus. The RNA samples were then subjected to real-time PCR analysis.

Cannulation and administration of guanabenz

For intracerebroventricular (icv) cannula implantation, mice were anesthetized by ip injection of tribromoethanol (250 mg/kg, Sigma-Aldrich) and placed in a stereotaxic apparatus (Stoelting, Wood Dale, IL, USA). The cannula (26 gauge) was implanted into the right lateral ventricle (1.0 mm lateral, 0.3 mm posterior, and 2.4 mm ventral to the bregma) according to the *Stereotaxic Mouse Brain Atlas* (Paxinos G and Franklin KBJ, 2001, Academic Press, San Diego, CA, USA) and secured to the skull with dental cement. After 7 days of recovery, mice were injected with vehicle (saline) or guanabenz (100 ng/2.5 μl). The food intake of the individually caged animals was

monitored for 24 h after the injection. For immunohistochemistry analysis, mice were sacrificed 1 h after the injection of guanabenz.

Immunohistochemistry (IHC)

Animals were deeply anesthetized with tribromoethanol and transcardially perfused with phosphate buffer (PB, 0.1 M, pH 7.4), followed by a fresh fixative of 4% paraformaldehyde in PB. Brains were post-fixed overnight at 4°C, sliced to a thickness of 50 μm using a vibratome (VT1000P; Leica Microsystems, wetzlar, Germany), and then washed several times in PB. Coronal brain sections containing the hypothalamic arcuate nucleus (ARC) were preincubated with 0.2% Triton X-100 (T8787, Sigma-Aldrich) in PB for 30 min to permeabilize the tissues and cells. After further washing with PB, the sections were incubated overnight at room temperature (RT) with rabbit anti-c-Fos antibody (1:1000; SC-52, Santacuz, California, CA, USA) and mouse anti-HA antibody (1:1,000; MMS-101R, BioLegend, San Diego, CA, USA). On the next day, sections were washed in PB. For immunofluorescence staining, sections were incubated with the following secondary antibodies for 2 h at room temperature: goat anti-rabbit Alexa Fluor 488 (1:500; A11008, Invitrogen, Carlsbad, CA, USA), goat anti-rabbit Alexa Fluor 594 (1:500; A11012, Invitrogen), goat anti-mouse Alexa Fluor 647 (1:500; A28181, Invitrogen) and goat anti-mouse Alexa Fluor 488 (1:500; A11001, Invitrogen). Stained brain sections were imaged using an FV-1200 confocal laser-scanning microscope (Olympus America, Inc., Center Valley, PA, USA). The number of c-Fos-positive cells in the hypothalamic ARC was counted by an unbiased observer.

Measurement of O_2 consumption, CO_2 production, and energy expenditure

Metabolic parameters, O_2 consumption (VO_2), CO_2 production (VCO_2), respiratory quotient (RQ) and energy expenditure, of mice were analyzed after guanabenz or vehicle injection using an indirect calorimetry system (Promethion, Sable Systems, Las Vegas, NV, USA). VO_2 and VCO_2 were measured at 10 min intervals for each mouse. Mice were acclimated in the chambers for 72 h prior to data collection. The average values during the light and dark periods were calculated. Data acquisition and instrument control were coordinated by MetaScreen software (version 2.3.12), and the obtained raw data were processed using ExpeData (version 1.9.14, Sable Systems).

Real-time PCR

RNA was isolated from hypothalami using Trizol reagent (Sigma-Aldrich) or immunoprecipitation with HA antibody, as explained above, and reverse transcribed with MMLV reverse transcriptase (Beams Biotechnology, Gyeonggi-do, Korea). Gene expression was measured by real-time PCR using Evagreen qPCR Mastermix (TApplied Biological Materials Inc., Richmond, BC, Canada). The primers used were as follows: Dat sense primer, 5'-CGC CTA AGA AAA CCA TTT CC-3'; Dat antisense primer, 5'-GCT GGA ATG GCT GGA GAG-3'; Gfap sense primer, 5'-CAG ACT TTC TCC AAC CTC CAG-3'; Gfap antisense primer, 5'-AAT CTG GTG AGC CTG TAT TGG-3'; α_{2A} adrenergic receptor sense primer, 5'-CAA GAT CAA CGA GAA GT-3'; α_{2A} adrenergic receptor antisense primer, 5'-GTG CGA CGC YYG ATC T-3'; α_{2B} adrenergic receptor sense primer, 5'-GAC GAG GTC TCG GAG CTA A-3'; α_{2B} adrenergic receptor antisense primer, 5'-GCC TCT CCG ACA GAA GTA A-3'; α_{2C} adrenergic receptor sense primer, 5'-GTG CGG CCT CGA TGA-3'; α_{2C} adrenergic

receptor antisense primer, 5'-CTT GGC CAC GCG GTA GAT-3'; L19 sense primer, 5'-GGT GAC CTG GAT GAG AAG GA-3'; L19 antisense primer, 5'-TTC AGC TTG TGG ATG TGC TC-3'. Real-time PCR was performed using the StepOnePlus™ Real-Time PCR System (Applied Biosystems, Foster City, CA, USA) for ~40 cycles. Relative mRNA expression was normalized with the L19 mRNA level and calculated using the $2^{-\Delta\Delta CT}$ method [21].

Electrophysiology

Whole-cell patch-clamp recordings from DAT-positive cells with tdTomato signals maintained in hypothalamic slice. The brains were removed and immediately submerged in ice-cold, carbogen-saturated (95% O_2, 5% CO_2) sucrose solution containing the following (in mM): 75 sucrose, 2.5 KCl, 7 $MgCl_2$, 0.5 $CaCl_2$, 1.3 NaH_2PO_4, 25 $NaHCO_3$, 25 glucose, pH 7.3. Hypothalamic coronal sections (300 μm) were cut in sucrose solution using the vibratome. The slices were placed in a holding chamber filled with gassed, artificial CSF (ACSF) (95% O_2, 5% CO_2) that contains the following (in mM): 125 NaCl, 2.5 KCl, 1 $MgCl_2$, 2 $CaCl_2$, 1.3 NaH_2PO_4, 25 $NaHCO_3$, and 25 glucose, pH 7.3 and then incubated at room temperature for at least 1 h before recording. Slices were transferred to a recording chamber and bathed with continuously bubbled ACSF (30–32°C) at a flow rate of ~3 ml/min.

Whole-cell patch-clamp recordings were performed using pipettes with 4–6 MΩ resistance after filling with internal solution. Recording pipettes were made of borosilicate glass (World Precision Instruments, Sarasota, FL, USA) using a PC-10 vertical puller (Narishige, Tokyo, Japan). The internal solution containing the followings (in mM): 135 potassium gluconate, 0.5 EGTA, 10 HEPES, 2 Mg-ATP, 0.3

Na_2-GTP and 10 phosphocreatine, pH 7.3 with KOH. DAT-positive cells in the arcuate nucleus were identified under tdTomato signals, and then differential interference contrast (DIC) was used to get a seal in these cells. After a gigaohm seal was obtained, a gentle negative pressure was applied to break through to the whole-cell configuration. Guanabenz (100 nM) was added to ACSF and perfused for 3~5 min into the recording chamber. All recordings were performed with a Multiclamp 700B amplifier (Molecular Devices, Sunnyvale, CA, USA). Data were collected with pCLAMP software (Molecular Devices). Mean ongoing firing activity and membrane potential values were calculated using Clampfit (Axon Instruments Inc, Union City, CA, USA) software.

Statistical analyses

Statistical analyses were performed in GraphPad Prism 5 software (GraphPad Software, San Diego, CA, USA). All data are expressed as the mean ± SEM. The statistical significance between two groups was analyzed by unpaired Student's t-test.

Results

Effect of guanabenz on feeding behavior and hypothalamic neuronal activity

To assess the central role of guanabenz in energy balance, mice were injected with guanabenz (100 ng/2.5 μl) into the lateral ventricle. Administration of guanabenz induced a significant increase in food intake until 6 h after injection (Figure 1A). Along with the difference in food intake, the body weight was increased by administration of guanabenz compared to vehicle until 6 h after injection (Figure 1B).

Since the arcuate nucleus (ARC) of the hypothalamus is a major region for the central control of feeding behavior, I determined the neuronal activity in ARC after administration of guanabenz. Interestingly, activation of c-Fos, a molecular marker for the neuronal activity, in the ARC of hypothalamus was significantly enhanced by administration of guanabenz compared to vehicle at 1 h after administration (Figure 1C, D). Collectively, these observations suggest that central administration of guanabenz affects the feeding as well as hypothalamic neuronal activity.

Central administration of guanabenz stimulates energy expenditure

Because food intake was acutely increased by icv treatment with guanabenz, I investigated the effect of guanabenz on the energy expenditure using indirect calorimetry. The mice given guanabenz had increased the VO_2 (Figure 2A, B), VCO_2 (Figure 2C, D), respiratory quotient (RQ) (Figure 2E, F) and energy expenditure (Figure 2G) for 3 h after injection. However, these metabolic parameters did not show any difference with vehicle at 6 h after administration of guanabenz. These observations demonstrate that central administration of guanabenz acutely affects the physiological energy balance through energy expenditure.

Guanabenz does not affect the hypothalamic AgRP and POMC neuronal activity

It has been well established that hypothalamic AgRP and POMC neurons primarily regulate feeding behavior and energy expenditure through sensing the whole-body energy condition [1-3]. Therefore, I investigated the activation of hypothalamic AgRP and POMC neurons 1 h after administration of guanabenz. Interestingly, activation of c-Fos in AgRP and POMC neurons did not show any difference with vehicle after administration of guanabenz (Figure 3A-D). These results indicate that central administration of guanabenz did not directly cause change of AgRP and POMC neuronal activity.

Hypothalamic dopaminergic neurons are activated by administration of guanabenz

As shown in Figure 1, central administration of guanabenz significantly increased the hypothalamic neuronal activity. However, activities of POMC and AgRP neurons were not stimulated by guanabenz. Accordingly, I investigated the change of dopaminergic neuronal activity in the ARC after administration of guanabenz. Because guanabenz stimulates the α_{2A} adrenergic receptor, I identified the expression of α_{2A} adrenergic receptor in the dopaminergic neurons in the ARC using a Ribo-Tag system of transgenic (*DAT-Cre;Rpl22*^{HA}) mice that express HA-tagged ribosomal protein Rpl22 in the cells expressing dopamine transporter (DAT). The IHC analysis identified specific HA signals in the DAT-positive cells (Figure 4A). Real-time PCR revealed that α_{2A} adrenergic receptor and α_{2C} adrenergic receptor were expressed in DAT-positive cells in the hypothalamic ARC (Figure 4B).

To identify changes in dopaminergic neuronal activity by guanabenz, I analyzed the activation of c-Fos in the hypothalamic DAT-positive cells after administration of guanabenz. Interestingly, c-Fos activation in DAT-positive cells was significantly increased by administration of guanabenz compared to vehicle (Figure 4C, D). To further verify if guanabenz causes an enhanced dopaminergic neuronal activity in the hypothalamus, electrical activity of DAT-positive cells was measured by whole-cell recordings on the hypothalamic slices containing DAT-positive cells that express tdTomato signals (Figure 4E). DAT-positive cells in the hypothalamus revealed a strong depolarization in response to guanabenz (100 nM) compared to aCSF (Figure 4F). Moreover, increased resting membrane potential and firing rate of DAT-positive cells were observed by guanabenz compared to vehicle (Figure 4G, F). Collectively, these findings suggest that central administration of guanabenz stimulates the hypothalamic dopaminergic neurons, and then may affect the feeding behavior.

Figures

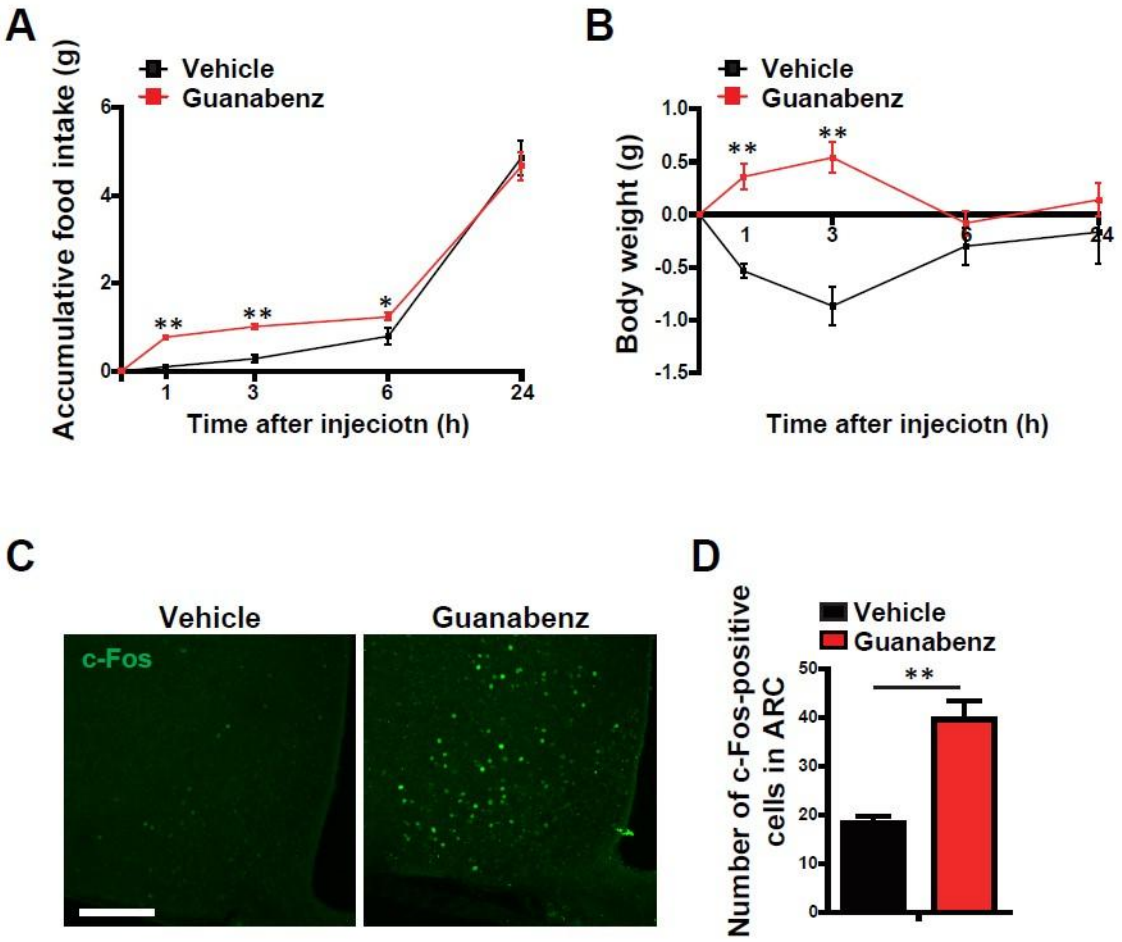

Figure 1. Guanabenz affects food intake, body weight and hypothalamic neuronal activity.

(A, B) Effect of guanabenz on food intake and body weight. Food intake (A) and body weight (B) were measured for 24 h after icv-injection with guanabenz (100 ng/2.5 μl) or vehicle (n=4/group). (C, D) Representative images (C) and calculated data (D) show the c-Fos positive neurons in the hypothalamic arcuate nucleus (ARC) after injection of guanabenz (n=6 sections of 2 mice/group). Data are presented as mean ± SEM. $^{*}p<0.05$ and $^{**}p<0.01$. Scale bar = 100 μm.

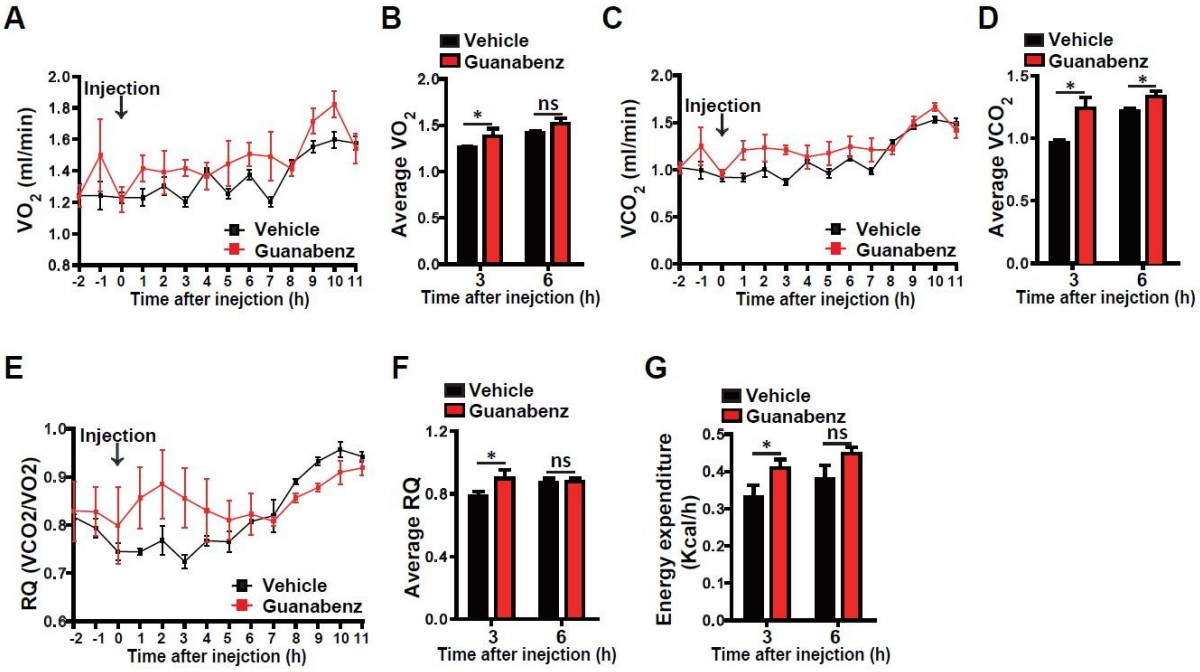

Figure 2. Effect of guanabenz on energy expenditure.

To identify whether guanabenz affects the energy expenditure, mice Ire subjected to measurement of metabolic parameters after administration of guanabenz. Indirect calorimetry measurements were performed in metabolic cages to determine changes in the oxygen consumption (VO2) (A, B), carbon dioxide generation (VCO2) (C, D), respiratory quotient (RQ) (E, F) and energy expenditure (G, n=6/group). Data are presented as mean ± SEM. $^{*}p<0.05$. ns, not significant.

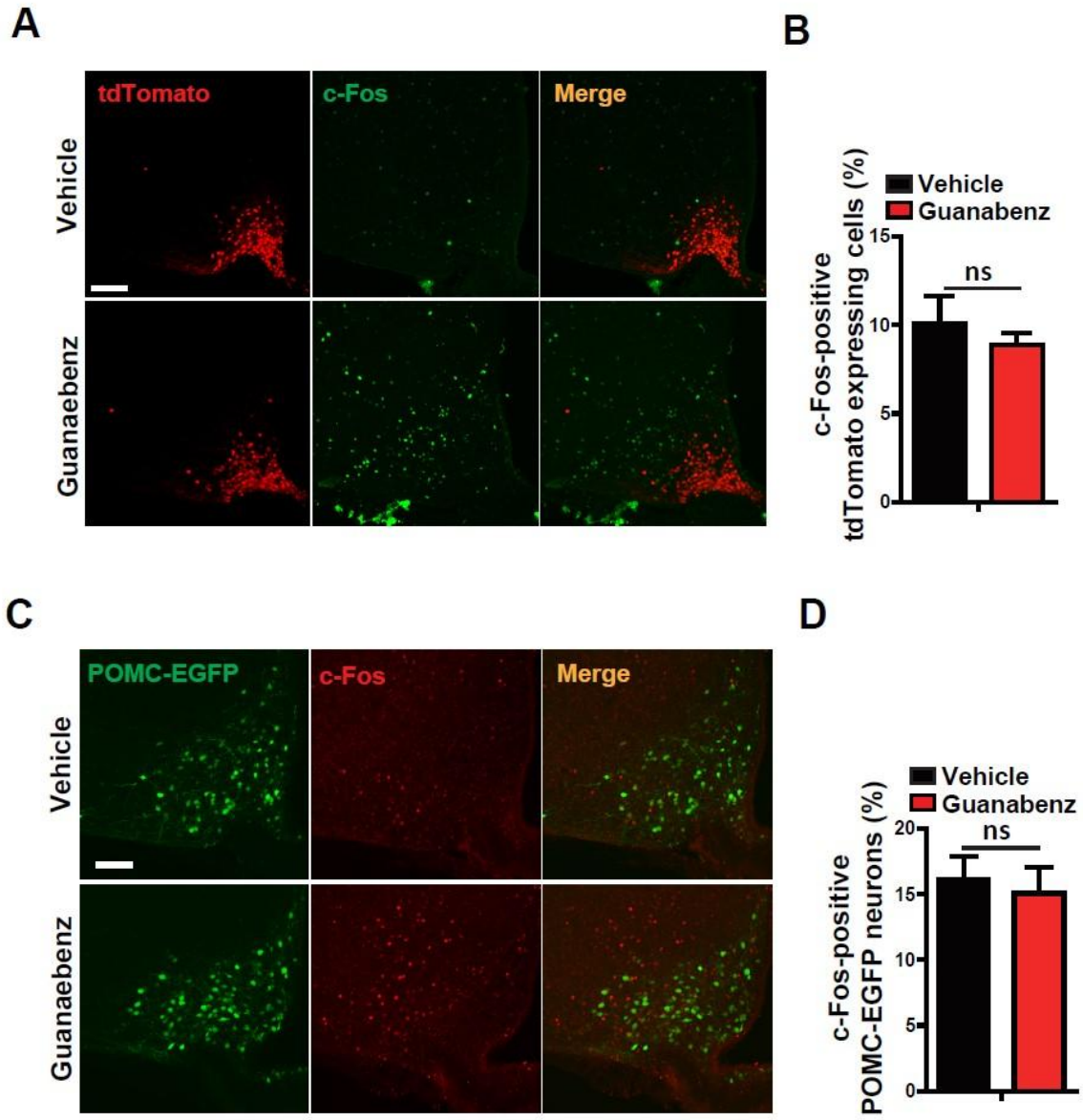

Figure 3. Guanabenz does not affect the hypothalamic AgRP and POMC neuronal activity.

To identify the effect of guanabenz on AgRP and POMC neurons, c-Fos immunoreactivity was measured by immunohistochemistry after administration of guanabenz. (A, B) Representative images (A) and calculated data (B) reveal that c-Fos positive AgRP neurons expressing tdTomato signals Ire not changed by

guanabenz compared to vehicle (n=4 sections of 2 mice/group). (C, D) Representative images (C) and calculated data (D) show the change of c-Fos positive POMC neurons expressing EGFP after administration of guanabenz or vehicle (n=4 sections of 2 mice/group). Data are presented as mean ± SEM. ns, not significant.

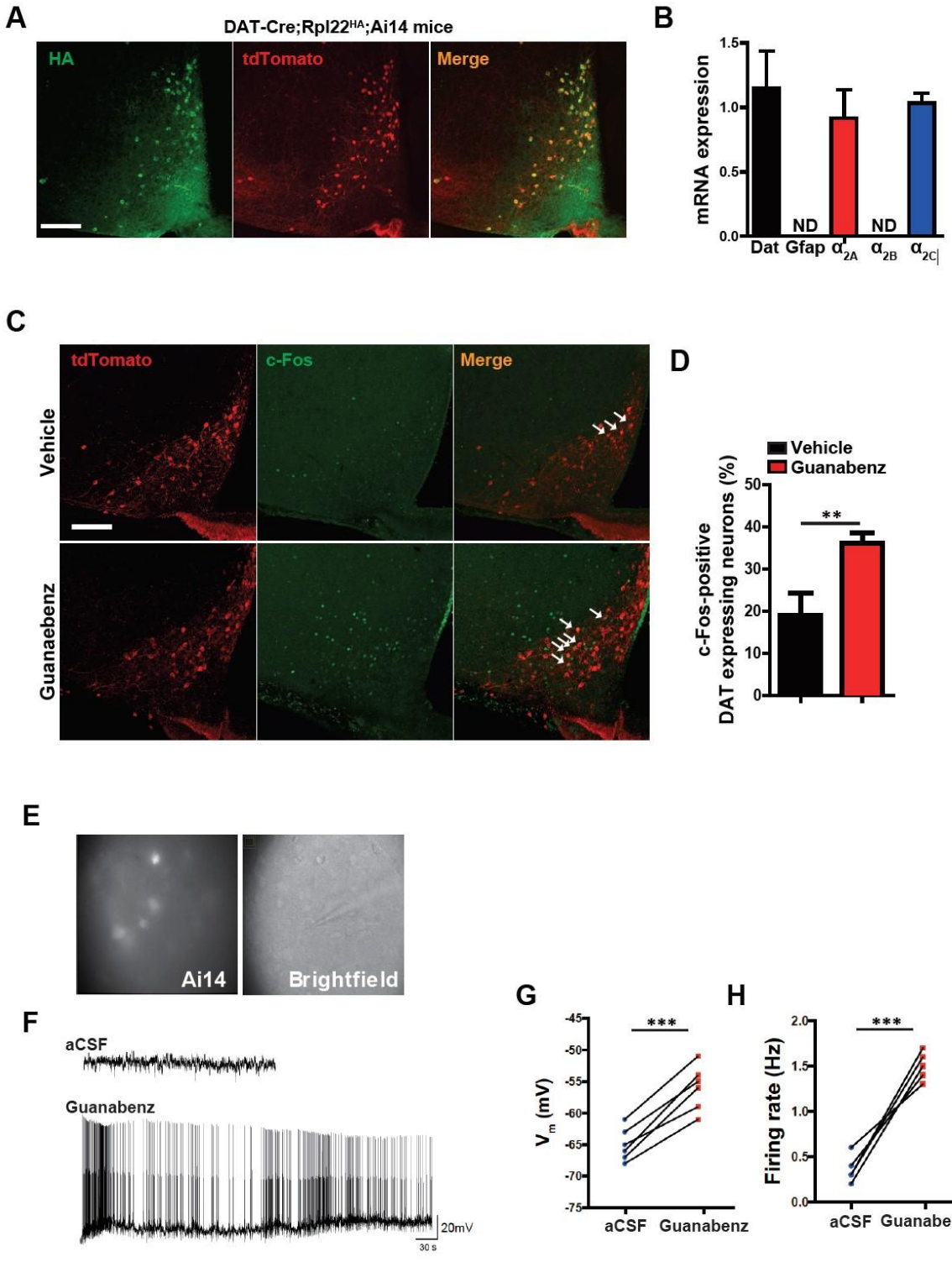
A
DAT-Cre;Rpl22HA;Ai14 mice
HA
tdTomato
Merge
B
mRNA expression
1.5
1.0
0.5
0.0
ND
ND
Dat
Gfap
α2A
α2B
α2C
C
tdTomato
c-Fos
Merge
Vehicle
Guanaebenz
D
Vehicle
Guanabenz
c-Fos-positive DAT expressing neurons (%)
50
40
30
20
10
0
**
E
Ai14
Brightfield
F
aCSF
Guanabenz
20mV
30 s
G
***
Vm (mV)
-45
-50
-55
-60
-65
-70
-75
aCSF
Guanabenz
H
***
Firing rate (Hz)
2.0
1.5
1.0
0.5
0.0
aCSF
Guanabenz

Figure 4. Hypothalamic DAT-positive cells are activated by central administration of guanabenz.

To investigate the expression of genes in dopamine transporter (DAT)-positive cells specifically using Ribo-Tag system, transgenic mice (*Rpl22*^{HA}) expressing HA-tagged Rpl22 were crossed with *DAT-Cre* mice, which resulted in generation of *DAT-Cre*;*Rpl22*^{HA} mice. (A, B) *DAT-Cre*;*Rpl22*^{HA} mice were bred with Ai14 reporter mice for detection of DAT-positive cells. (A) Representative images showing co-expression of DAT-positive cell-specific tdTomato signals and HA signals in the hypothalamic ARC of *DAT-Cre*;*Rpl22*^{HA}*;Ai14* mice. (B) Real-time PCR analyses of RNA samples (immunoprecipitated with HA antibody) were performed to detemine the expression of Dat, Gfap, α_{2A}, α_{2B} and α_{2C} adrenergic receptors from hypothalamic extracts of *DAT-Cre*;*Rpl22*^{HA} mice (n=3/group). (C, D) Representative images (C) and calculated data (D) reveal that c-Fos positive DAT-expressing cells were increased by guanabenz compared to vehicle (n=6 sections of 3 mice/group). (E-H) To identify changes in electrical membrane properties of the DAT-positive cells after treatment of guanabenz, hypothalamic slices were examined by patch-clamp recording. (E) Bright-field and tdTomato (Ai14) signals during acquisition of a whole-cell recording. (F) Treatment of guanabenz (100 nM) produced high frequency spikes in DAT-positive cells. (G, F) Guanabenz induced a greater increase in resting membrane potentials (mV) (G) and firing rate (F) in DAT-positive cells than vehicle (n=5 cells/4 mice/group). Data are presented as mean ± SEM. $^{**}p<0.01$ and $^{***}p<0.001$. Scale bar = 100 μm.

Discussion

In the present study, I found that central administration of guanabenz acutely influenced the food intake and the energy expenditure. Furthermore, guanabenz induced the activation of hypothalamic dopaminergic neurons. The current observations demonstrate a novel function of guanabenz is in the control of feeding and energy expenditure through regulation of hypothalamic dopaminergic neuronal activity.

In this study, I identified the function of guanabenz in feeding and energy balance. Interestingly, central administration of guanabenz increased food intake and body weight for 3 h after injection. Moreover, neuronal activity in hypothalamic ARC was significantly increased at 1 h after administration of guanabenz. Therefore, central administration of guanabenz is likely to be involved in feeding control through regulation of neuronal activity in hypothalamic ARC. Furthermore, respiratory quotient (RQ) and energy expenditure were increased for 3 h after administration of guanabenz. However, guanabenz did not show any difference in food intake, RQ and energy expenditure compared to vehicle for 6 h after injection. These results might be due to that central administration of guanabenz acutely affected neuronal activity for the food intake. However, this possibility must be studied in detail in future. Also, I could not exclude a possible contribution of guanebenz in other sites of hypothalamus. Therefore, further studies are required to identify the effect of guanabenz in several hypothalamic nuclei including PVN, VMH and LH.

The circuit of hypothalamic AgRP and POMC neurons is important in energy homeostasis through control of food intake and energy expenditure [1, 3]. Recently, it is reported that adrenergic receptors are differentially expressed between AgRP and

POMC neurons, and noradrenaline modulates the AgRP and POMC neuronal activity through adrenergic recepors [4]. In current study, I observed that administration of guanabenz did not directly induce any change in AgRP and POMC neuronal activity. These results might indicate that guanabenz modulates food intake through hypothalamic cells other than AgRP and POMC neurons. Interestingly, a recent report showed that hypothalamic dopaminergic neurons are excited by ghrelin and play an orexigenic role in energy homeostasis [18]. In this study, α_{2A}-adrenergic receptors were expressed in hypothalamic dopaminergic neurons. Furthermore, I found that dopaminergic neurons in hypothalamic ARC were stimulated by administration of guanabenz. In line with previous report, these results indicate that guanabenz induced hypothalamic dopaminergic neurons and thus indirectly affected food intake and energy expenditure.

Further studies are certainly required to uncover detailed cellular and molecular mechanisms for function of guanabenz in hypothalamic dopaminergic neurons on regulation of feeding. It is also important in understanding of unidentified mechanisms in the energy homeostasis to clarify whether α_{2A}-adrenergic receptor in dopaminergic neurons affects other neuronal populations in the hypothalamus. Since dopaminergic neurons locate the midbrain as well as hypothalamus, further studies are required to identify the effect of guanabenz in dopaminergic neurons of midbrain.

In summary, this study identified function of guanabenz for the regulation of the feeding behavior and energy expenditure, which highlights contribution of guanabenz to dopaminergic neuronal activity in the hypothalamus.

References

1. Williams KW, Elmquist JK: From neuroanatomy to behavior: central integration of peripheral signals regulating feeding behavior. *Nat Neurosci* 2012, 15:1350-1355.
2. Balthasar N, Dalgaard LT, Lee CE, Yu J, Funahashi H, Williams T, Ferreira M, Tang V, McGovern RA, Kenny CD, et al: Divergence of melanocortin pathways in the control of food intake and energy expenditure. *Cell* 2005, 123:493-505.
3. Roh E, Song DK, Kim MS: Emerging role of the brain in the homeostatic regulation of energy and glucose metabolism. *Exp Mol Med* 2016, 48:e216.
4. Paeger L, Karakasilioti I, Altmuller J, Frommolt P, Bruning J, Kloppenburg P: Antagonistic modulation of NPY/AgRP and POMC neurons in the arcuate nucleus by noradrenalin. *Elife* 2017, 6.
5. Giovannitti JA, Jr., Thoms SM, Crawford JJ: Alpha-2 adrenergic receptor agonists: a review of current clinical applications. *Anesth Prog* 2015, 62:31-39.
6. MacDonald E, Kobilka BK, Scheinin M: Gene targeting--homing in on alpha 2-adrenoceptor-subtype function. *Trends Pharmacol Sci* 1997, 18:211-219.
7. Khasar SG, Green PG, Chou B, Levine JD: Peripheral nociceptive effects of alpha 2-adrenergic receptor agonists in the rat. *Neuroscience* 1995, 66:427-432.
8. Buerkle H: Peripheral anti-nociceptive action of alpha2-adrenoceptor agonists. Best Pract Res Clin Anaesthesiol 2000,14:411-418.
9. Gyires K, Zadori ZS, Torok T, Matyus P: alpha(2)-Adrenoceptor subtypes-mediated physiological, pharmacological actions. *Neurochem Int* 2009, 55:447-453.
10. Gehr M, MacCarthy EP, Goldberg M: Guanabenz: a centrally acting, natriuretic antihypertensive drug. *Kidney Int* 1986, 29:1203-1208.

11. Sica DA: Centrally acting antihypertensive agents: an update. *J Clin Hypertens (Greenwich)* 2007, 9:399-405.
12. Hall JE, Brands MW, Hildebrandt DA, Kuo J, Fitzgerald S: Role of sympathetic nervous system and neuropeptides in obesity hypertension. *Braz J Med Biol Res* 2000, 33:605-618.
13. Messina G, De Luca V, Viggiano A, Ascione A, Iannaccone T, Chieffi S, Monda M: Autonomic nervous system in the control of energy balance and body weight: personal contributions. *Neurol Res Int* 2013, 2013:639280.
14. Volkow ND, Wang GJ, Baler RD: Reward, dopamine and the control of food intake: implications for obesity. *Trends Cogn Sci* 2011, 15:37-46.
15. Palmiter RD: Is dopamine a physiologically relevant mediator of feeding behavior? *Trends Neurosci* 2007, 30:375-381.
16. Meguid MM, Fetissov SO, Varma M, Sato T, Zhang L, Laviano A, Rossi-Fanelli F: Hypothalamic dopamine and serotonin in the regulation of food intake. *Nutrition* 2000, 16:843-857.
17. Leinninger GM, Jo YH, Leshan RL, Louis GW, Yang H, Barrera JG, Wilson H, Opland DM, Faouzi MA, Gong Y, et al: Leptin acts via leptin receptor-expressing lateral hypothalamic neurons to modulate the mesolimbic dopamine system and suppress feeding. *Cell Metab* 2009, 10:89-98.
18. Zhang X, van den Pol AN: Hypothalamic arcuate nucleus tyrosine hydroxylase neurons play orexigenic role in energy homeostasis. *Nat Neurosci* 2016, 19:1341-1347.

19. Sanz E, Yang L, Su T, Morris DR, McKnight GS, Amieux PS: Cell-type-specific isolation of ribosome-associated mRNA from complex tissues. *Proc Natl Acad Sci U S A* 2009, 106:13939-13944.
20. Kang SS, Ebbert MTW, Baker KE, Cook C, Wang X, Sens JP, Kocher JP, Petrucelli L, Fryer JD: Microglial translational profiling reveals a convergent APOE pathway from aging, amyloid, and tau. *J Exp Med* 2018, 215:2235-2245.
21. Livak KJ, Schmittgen TD: Analysis of relative gene expression data using real-time quantitative PCR and the 2(-Delta Delta C(T)) Method. *Methods* 2001, 25:402-408.